Effect of a small curvature of the surfaces on microscale lubrication of a gas for large Knudsen numbers

Toshiyuki Doi ®[*]

Department of Applied Mathematics and Physics, Tottori University, Tottori 680-8552, Japan

Lubrication flow of a gas in a microscale gap between coaxial circular cylinders is studied on the basis of kinetic theory. The stationary inner cylinder is a Maxwell-type boundary with a nonuniform accommodation coefficient in the circumferential direction, and the outer cylinder is a diffuse reflection boundary rotating at a constant speed. The dimensionless curvature, defined as the gap size divided by the radius of the inner cylinder, is small, and the Knudsen number based on the gap size is arbitrary. The Boltzmann equation is studied analytically using the slowly varying approximation, with special attention being paid to the characteristics of the equation. Two macroscopic lubrication models of the Reynolds-type equations are derived: one consisting of the solutions for plane Couette and Poiseuille flows (plane lubrication model), and the other consisting of cylindrical Couette flow and a curved Poiseuille flow (improved lubrication model). For an assessment of the models, a direct numerical analysis of the flow is also conducted for the Bhatnagar-Gross-Krook-Welander kinetic equation using a hybrid finite-difference method. It is demonstrated that the use of the plane lubrication model leads to a non-negligible error when the Knudsen number is sufficiently large. This error is caused by neglect of the fact that the number of molecules arriving from the outer cylinder is greater than that from the inner one by an amount proportional to the square root of the dimensionless curvature. It is also demonstrated that the improved lubrication model provides an excellent approximation to the direct numerical solution over the whole range of the Knudsen number.

I. INTRODUCTION

Flows of a gas in microscale gaps play important roles in lubrication in microelectromechanical systems [1–5]. An example is lubrication between a magnetic disk and a head slider in a hard disk drive. When the gap size is comparable with the mean-free path of the gas, conventional lubrication theory based on continuum fluid dynamics is inapplicable. Instead, an approach based on kinetic theory is necessary. The theory of microscale lubrication has been studied extensively on the basis of kinetic theory [6–12]. In the 1980s, a generalized Reynolds equation applicable to an arbitrary Knudsen number has been derived [8], where the Knudsen number is defined as the mean-free path divided by the gap size; a more systematic derivation is given in Ref. [12]. Some recent extensions can be found, for example, in Refs. [13,14].

Flows in narrow gaps between bodies with curved surfaces occur in lubrication between journals and bearings in micromachines. In these systems, the ratio of gap size to radius of curvature is usually small; we shall call this ratio the dimensionless curvature and denote it by ε. A Reynolds equation taking the curvature effect into account has been derived from the

---

[*]doi@tottori-u.ac.jp

Navier-Stokes equation in Ref. [15]. For microscale lubrication, the Boltzmann equation written in a general orthogonal curvilinear coordinate system was analyzed using the slowly varying approximation up to the first order of ε in Ref. [12], and the generalized Reynolds equation has been derived. The error in this equation is supposed to be of $O(\varepsilon^2)$. However, for a gas at a large Knudsen number, there is a possibility that the error could be much greater, for the following reason.

In the slowly varying approximation, the flow is considered on the scale of the gap size, and so the channel walls can be taken to be nearly parallel planes. The solution is then approximated locally by a linear combination of Poiseuille and Couette flows of a rarefied gas between parallel planes. However, it is known in rarefied gas dynamics that when the Knudsen number is large, Poiseuille and Couette flows in a slightly curved channel are considerably different from those in a straight channel. For example, at infinite Knudsen number, the flow velocity in plane Couette flow is independent of the position, whereas it is position-dependent in cylindrical Couette flow. This dependence in the cylindrical case arises because the number of molecules arriving at a point in the gas from each cylindrical wall depends on the position of the point; the number of molecules from the inner cylinder increases in approaching this cylinder because the range of directions of molecular velocities from this cylinder increases. By an elementary estimate, the number of molecules arriving from the outer cylinder is greater than that from the inner one by an amount proportional to $O(\varepsilon^{1/2})$. Because the square root of ε is much larger than ε^2, the replacement of the slightly curved flow by a plane flow may cause a non-negligible error much larger than ε^2. Therefore, careful attention should be paid to the influence of small curvature on a lubrication flow when the Knudsen number is large.

In this paper, we study the influence of small curvature on the lubrication flow of a gas in a microscale gap on the basis of kinetic theory. To make the essential points clear, we study the simplified case of an annulus between coaxial circular cylinders. The inner cylinder, which is at rest, is a Maxwell-type boundary whose accommodation coefficient is nonuniform in the circumferential direction. The outer cylinder is a diffuse reflection boundary and rotates at a constant speed. The nonuniform accommodation coefficient is introduced to induce a pressure variation in place of an eccentricity of the cylinders. The dimensionless curvature ε, i.e., the gap size divided by the radius of the inner cylinder, is small, and the Knudsen number based on the gap size is arbitrary. We study the solution of the Boltzmann equation analytically using the slowly varying approximation [12], with special attention to the trajectories of the molecules arriving from each cylinder. An improved lubrication model, which takes the curvature effect into account, is derived. A direct numerical analysis of the flow is also conducted for the Bhatnagar-Gross-Krook-Welander (BGKW) kinetic equation [16,17] using a hybrid finite-difference method as a reference for an assessment of the lubrication model. The main goals of this paper are as follows: (1) to demonstrate that the lubrication model that consists of plane Poiseuille and Couette flows causes a non-negligible error of $O(\varepsilon^{1/2})$ when the Knudsen number is sufficiently large and (2) to demonstrate that the improved lubrication model exhibits excellent agreement with the direct numerical solution uniformly over the whole range of the Knudsen number.

II. PROBLEM AND BASIC EQUATION

A. Problem

Consider a rarefied gas in the annulus between coaxial circular cylinders at $r = r_1$ and $r = r_2 (r_2 > r_1)$ as shown in Fig. 1(a), where (r, θ, z) is the spatial cylindrical coordinate system. The inner cylinder at rest is a Maxwell-type boundary whose accommodation coefficient α_a is a function of θ as shown, for example, in Fig. 1(b). The outer cylinder is a diffuse reflection boundary and rotates at a constant circumferential velocity v_w. The temperature of the cylinders is a constant T_0. The dimensionless curvature ε is defined by $\varepsilon = D/r_1$ and the Knudsen number Kn is defined by Kn $= \ell/D$, where $D = r_2 - r_1$ is the gap size and ℓ is the mean-free path of the gas in the equilibrium
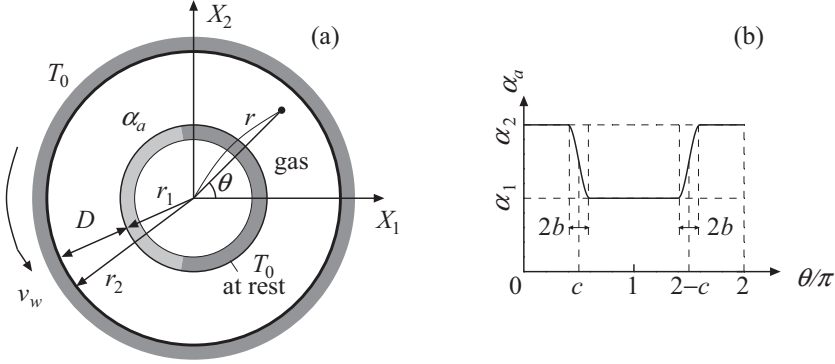
FIG. 1. Schematic of the system. (a) Schematic of the system and the coordinate system and (b) distribution of the accommodation coefficient α_a. In panel (b), the graph is plotted for the function (53) with $\alpha_1/\alpha_2 = 0.5$, $b = 0.1$, and $c = 0.5$.

state at rest with the temperature T_0 and the average density ρ_0 of the gas. Let ε be small, and let the speed of rotation also be small. To be specific,

$$\frac{D}{r_1} = \varepsilon \ll 1 \quad \text{and} \quad \frac{v_w}{(2RT_0)^{1/2}} = \hat{v}_w = \varepsilon u_w, \tag{1}$$

where R is the specific gas constant, i.e., the Boltzmann constant divided by the mass of a molecule, and u_w is a constant of the order of unity. The Knudsen number $\mathrm{Kn} = \ell/D$ is arbitrary. We study the time-independent and axially uniform behavior of the gas on the basis of the Boltzmann equation.

B. Basic equation

In this paper, we use the following dimensionless variables. Let $\hat{r}$, ζ_i $(i = r, \theta, z)$, and $\hat{f}(\hat{r}, \theta, \zeta_r, \zeta_\theta, \zeta_z)$ be the dimensionless variables for the radial coordinate r, the molecular velocity ξ_i, and the velocity distribution function f defined by

$$\hat{r} = \frac{r}{D}, \quad \zeta_i = \frac{\xi_i}{(2RT_0)^{1/2}}, \quad \hat{f} = \frac{f}{\rho_0(2RT_0)^{-3/2}}. \tag{2}$$

The ζ_i is also denoted by $\boldsymbol{\zeta}$.

The Boltzmann equation in the time-independent state for the axially uniform case is written as

$$\zeta_r \frac{\partial \hat{f}}{\partial \hat{r}} + \frac{\zeta_\theta}{\hat{r}} \frac{\partial \hat{f}}{\partial \theta} + \frac{\zeta_\theta}{\hat{r}} \left(\zeta_\theta \frac{\partial \hat{f}}{\partial \zeta_r} - \zeta_r \frac{\partial \hat{f}}{\partial \zeta_\theta} \right) = \frac{1}{k} \hat{J}(\hat{f}, \hat{f}), \tag{3}$$

where $k = (\sqrt{\pi}/2)\mathrm{Kn}$. The $\hat{J}(\cdot, \cdot)$ is the dimensionless collision integral defined by

$$\hat{J}(\hat{f}, \hat{g}) = \frac{1}{2} \iint [\hat{f}(\boldsymbol{\zeta}'_*)\hat{g}(\boldsymbol{\zeta}') + \hat{f}(\boldsymbol{\zeta}')\hat{g}(\boldsymbol{\zeta}'_*) - \hat{f}(\boldsymbol{\zeta}_*)\hat{g}(\boldsymbol{\zeta}) - \hat{f}(\boldsymbol{\zeta})\hat{g}(\boldsymbol{\zeta}_*)]\hat{B} \, d\Omega(\mathbf{e})\mathbf{d}\boldsymbol{\zeta}_*,$$

$$\boldsymbol{\zeta}' = \boldsymbol{\zeta} + [\mathbf{e} \cdot (\boldsymbol{\zeta}_* - \boldsymbol{\zeta})]\mathbf{e}, \quad \boldsymbol{\zeta}'_* = \boldsymbol{\zeta}_* - [\mathbf{e} \cdot (\boldsymbol{\zeta}_* - \boldsymbol{\zeta})]\mathbf{e}, \tag{4}$$

where $\mathbf{e}$ is a unit vector, $d\Omega(\mathbf{e})$ is the solid-angle element in the direction of $\mathbf{e}$, and $\mathbf{d}\boldsymbol{\zeta}_* = d\zeta_{r*} \, d\zeta_{\theta*} \, d\zeta_{z*}$. The $\hat{B}$ is a function of $|\mathbf{e} \cdot (\boldsymbol{\zeta}_* - \boldsymbol{\zeta})|/|\boldsymbol{\zeta}_* - \boldsymbol{\zeta}|$ and $|\boldsymbol{\zeta}_* - \boldsymbol{\zeta}|$, and its functional form is determined by the molecular model. In Eq. (4), the arguments of the spatial variables $\hat{r}$ and θ are common and are omitted for simplicity. The integration in Eq. (4) is carried out over the entire direction of $\mathbf{e}$ and the entire space of $\boldsymbol{\zeta}$.

The boundary condition on the inner cylinder is the Maxwell-type condition given by

$$\hat{f}(\zeta_r) = [1 - \alpha_a(\theta)]\hat{f}(-\zeta_r) + \alpha_a(\theta)\hat{\sigma}_a E \quad (\hat{r} = 1/\varepsilon, \ \zeta_r > 0),$$

$$\hat{\sigma}_a = -2\sqrt{\pi} \int_{\zeta_r < 0} \zeta_r \hat{f} \mathbf{d}\zeta \quad (\hat{r} = 1/\varepsilon), \tag{5}$$

where $E = \pi^{-3/2} \exp(-\zeta^2)$, and $\hat{f}(\pm\zeta_r)$ in Eq. (5) is the abbreviation for $\hat{f}(\hat{r}, \theta, \pm\zeta_r, \zeta_\theta, \zeta_z)$. The boundary condition on the outer cylinder is given by

$$\hat{f} = \pi^{-3/2}\hat{\sigma}_b \exp\left(-\zeta_r^2 - (\zeta_\theta - \hat{v}_w)^2 - \zeta_z^2\right) \quad (\hat{r} = 1/\varepsilon + 1, \ \zeta_r < 0),$$

$$\hat{\sigma}_b = 2\sqrt{\pi} \int_{\zeta_r > 0} \zeta_r \hat{f} \mathbf{d}\zeta \quad (\hat{r} = 1/\varepsilon + 1). \tag{6}$$

The periodic boundary condition with respect to θ is given by

$$\hat{f}(\hat{r}, 0, \zeta_r, \zeta_\theta, \zeta_z) = \hat{f}(\hat{r}, 2\pi, \zeta_r, \zeta_\theta, \zeta_z) \quad (\zeta_\theta > 0), \tag{7}$$

$$\hat{f}(\hat{r}, 2\pi, \zeta_r, \zeta_\theta, \zeta_z) = \hat{f}(\hat{r}, 0, \zeta_r, \zeta_\theta, \zeta_z) \quad (\zeta_\theta < 0). \tag{8}$$

Finally from the definition of the average gas density ρ_0, we have

$$\int_0^{2\pi} d\theta \int_{1/\varepsilon}^{1/\varepsilon+1} d\hat{r}\hat{r} \int \hat{f}\mathbf{d}\zeta = \pi\left(\frac{2}{\varepsilon} + 1\right). \tag{9}$$

The macroscopic variables of the gas, i.e., the density ρ, the flow velocity v_i $(i = r, \theta)$, the temperature T, the pressure p, and the stress tensor p_{ij} $(j = r, \theta)$ are defined by the moments of the velocity distribution function f. The dimensionless variables $\hat{\rho} = \rho/\rho_0$, $\hat{v}_i = v_i/(2RT_0)^{1/2}$, $\hat{T} = T/T_0$, $\hat{p} = p/p_0$ $(p_0 = R\rho_0 T_0)$, and $\hat{p}_{ij} = p_{ij}/p_0$ are given by the moments of the dimensionless distribution function $\hat{f}$ as

$$\hat{\rho} = \int \hat{f}\mathbf{d}\zeta, \tag{10a}$$

$$\hat{v}_i = \frac{1}{\hat{\rho}} \int \zeta_i \hat{f}\mathbf{d}\zeta \quad (i = r, \theta), \tag{10b}$$

$$\hat{T} = \frac{2}{3\hat{\rho}} \int \left[(\zeta_r - \hat{v}_r)^2 + (\zeta_\theta - \hat{v}_\theta)^2 + \zeta_z^2\right]\hat{f}\mathbf{d}\zeta, \tag{10c}$$

$$\hat{p} = \hat{\rho}\hat{T}, \tag{10d}$$

$$\hat{p}_{ij} = 2 \int (\zeta_i - \hat{v}_i)(\zeta_j - \hat{v}_j)\hat{f}\mathbf{d}\zeta \quad (j = r, \theta). \tag{10e}$$

The force (F_1, F_2) acting on the inner cylinder per unit depth in the z direction is given by

$$\frac{1}{p_0 r_1}\begin{pmatrix} F_1 \\ F_2 \end{pmatrix} = -\int_0^{2\pi} \begin{pmatrix} \hat{p}_{rr}\cos\theta - \hat{p}_{\theta r}\sin\theta \\ \hat{p}_{rr}\sin\theta + \hat{p}_{\theta r}\cos\theta \end{pmatrix} d\theta \quad (\hat{r} = 1/\varepsilon), \tag{11}$$

where (F_1, F_2) are the components in the rectangular coordinates (X_1, X_2) in which X_1 points in the direction $\theta = 0$ [see Fig. 1(a)]. The torque N acting on the inner cylinder per unit depth is given by

$$\frac{N}{p_0 r_1^2} = -\int_0^{2\pi} \hat{p}_{\theta r} d\theta \quad (\hat{r} = 1/\varepsilon). \tag{12}$$

C. Some transformations

For a convenience of the analysis and numerical analysis, we introduce the change of independent variables from $\hat{r}$, ζ_r, and ζ_θ to y, ζ_ρ, and θ_ζ [18]:

$$\hat{r} = 1/\varepsilon + y, \quad \zeta_r = \zeta_\rho \cos\theta_\zeta, \quad \zeta_\theta = \zeta_\rho \sin\theta_\zeta, \tag{13}$$

where $0 < y < 1$ and $-\pi < \theta_\zeta \leqslant \pi$. In terms of y, ζ_ρ, and θ_ζ, the boundary value problem (3)–(9) is rewritten as follows. The Boltzmann equation is

$$\zeta_\rho \cos\theta_\zeta \frac{\partial \hat{f}}{\partial y} + \frac{\varepsilon\zeta_\rho \sin\theta_\zeta}{1+\varepsilon y} \frac{\partial \hat{f}}{\partial \theta} - \frac{\varepsilon\zeta_\rho \sin\theta_\zeta}{1+\varepsilon y} \frac{\partial \hat{f}}{\partial \theta_\zeta} = \frac{1}{k} \hat{J}(\hat{f}, \hat{f}). \tag{14}$$

The boundary conditions (5)–(8) and the subsidiary condition (9) are transformed into

$$\hat{f} = [1 - \alpha_a(\theta)]\hat{f}(\tilde{\theta}_\zeta) + \alpha_a(\theta)\hat{\sigma}_a E \quad (y = 0, \ \cos\theta_\zeta > 0), \tag{15}$$

$$\hat{f} = \pi^{-3/2}\hat{\sigma}_b \exp\left(-\zeta_\rho^2 + 2\varepsilon u_w \zeta_\rho \sin\theta_\zeta - \varepsilon^2 u_w^2 - \zeta_z^2\right) \quad (y = 1, \ \cos\theta_\zeta < 0), \tag{16}$$

$$\hat{\sigma}_a = -2\sqrt{\pi} \iiint_{\cos\theta_\zeta < 0} \zeta_\rho^2 \cos\theta_\zeta \hat{f} \, d\zeta_\rho \, d\theta_\zeta \, d\zeta_z \quad (y = 0),$$

$$\hat{\sigma}_b = 2\sqrt{\pi} \iiint_{\cos\theta_\zeta > 0} \zeta_\rho^2 \cos\theta_\zeta \hat{f} \, d\zeta_\rho \, d\theta_\zeta \, d\zeta_z \quad (y = 1),$$

$$\hat{f}(\hat{r}, 0, \zeta_r, \theta_\zeta, \zeta_z) = \hat{f}(\hat{r}, 2\pi, \zeta_r, \theta_\zeta, \zeta_z) \quad (\theta_\zeta > 0), \tag{17}$$

$$\hat{f}(\hat{r}, 2\pi, \zeta_r, \theta_\zeta, \zeta_z) = \hat{f}(\hat{r}, 0, \zeta_r, \theta_\zeta, \zeta_z) \quad (\theta_\zeta < 0), \tag{18}$$

$$\int_0^{2\pi} d\theta \int_0^1 dy \left(\frac{1}{\varepsilon} + y\right) \iiint \zeta_\rho \hat{f} \, d\zeta_\rho \, d\theta_\zeta \, d\zeta_z = \pi\left(\frac{2}{\varepsilon} + 1\right), \tag{19}$$

where $E = \pi^{-3/2} \exp(-\zeta_\rho^2 - \zeta_z^2)$ in the new variables. Here and in what follows, we use the convention that $\hat{f}(\hat{r}(y), \theta, \zeta_r(\zeta_\rho, \theta_\zeta), \zeta_\theta(\zeta_\rho, \theta_\zeta), \zeta_z)$ is simply written as $\hat{f}(y, \theta, \zeta_\rho, \theta_\zeta, \zeta_z)$ because no confusion will arise. In Eq. (15), $\hat{f}(\tilde{\theta}_\zeta)$ is an abbreviation for $\hat{f}(y, \theta, \zeta_\rho, \tilde{\theta}_\zeta, \zeta_z)$ and $\tilde{\theta}_\zeta = \pm\pi - \theta_\zeta$, depending on whether $\pm\theta_\zeta > 0$. The ranges of integration with respect to ζ_ρ, θ_ζ, and ζ_z are, respectively, $0 < \zeta_\rho < \infty$, $-\pi < \theta_\zeta < \pi$, and $-\infty < \zeta_z < \infty$ unless otherwise stated.

The macroscopic variables are

$$\hat{\rho} = \iiint \zeta_\rho \hat{f} \, d\zeta_\rho \, d\theta_\zeta \, d\zeta_z, \tag{20a}$$

$$\hat{v}_r = \frac{1}{\hat{\rho}} \iiint \zeta_\rho^2 \cos\theta_\zeta \hat{f} \, d\zeta_\rho \, d\theta_\zeta \, d\zeta_z, \tag{20b}$$

$$\hat{v}_\theta = \frac{1}{\hat{\rho}} \iiint \zeta_\rho^2 \sin\theta_\zeta \hat{f} \, d\zeta_\rho \, d\theta_\zeta \, d\zeta_z, \tag{20c}$$

$$\hat{T} = \frac{2}{3\hat{\rho}} \iiint \zeta_\rho\left[(\zeta_\rho \cos\theta_\zeta - \hat{v}_r)^2 + (\zeta_\rho \sin\theta_\zeta - \hat{v}_\theta)^2 + \zeta_z^2\right]\hat{f} \, d\zeta_\rho \, d\theta_\zeta \, d\zeta_z, \tag{20d}$$

$$\hat{p} = \hat{\rho}\hat{T}, \tag{20e}$$

$$\hat{p}_{rr} = 2 \iiint \zeta_\rho(\zeta_\rho \cos\theta_\zeta - \hat{v}_r)^2 \hat{f} \, d\zeta_\rho \, d\theta_\zeta \, d\zeta_z, \tag{20f}$$
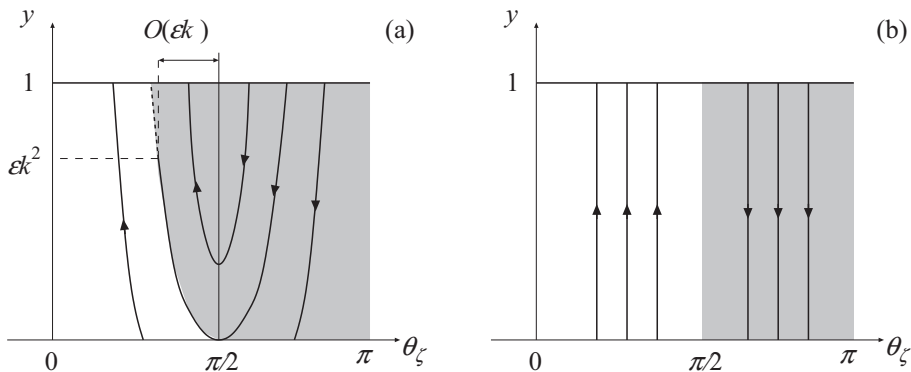
FIG. 2. Characteristics, or the trajectories of collisionless molecules, in the θ_ζ-y plane ($\theta_\zeta > 0$). (a) Projection of the characteristics of Eq. (14) onto the θ_ζ-y plane and (b) those of Eq. (14) in which the curvature term is omitted. The shaded region represents the molecular trajectories arriving from the rotating outer cylinder, and the unshaded region represents those from the inner cylinder at rest. In panel (a), the velocity distribution function is discontinuous across their boundary (22) with const = 1. In (a), $O(\varepsilon k)$ reduces to $O(\varepsilon^{1/2})$ when $\varepsilon k^2 = O(1)$.

$$\hat{p}_{r\theta} = \hat{p}_{\theta r} = 2 \iiint \zeta_\rho (\zeta_\rho \cos\theta_\zeta - \hat{v}_r)(\zeta_\rho \sin\theta_\zeta - \hat{v}_\theta)\hat{f} \, d\zeta_\rho \, d\theta_\zeta \, d\zeta_z, \tag{20g}$$

$$\hat{p}_{\theta\theta} = 2 \iiint \zeta_\rho (\zeta_\rho \sin\theta_\zeta - \hat{v}_\theta)^2 \hat{f} \, d\zeta_\rho \, d\theta_\zeta \, d\zeta_z. \tag{20h}$$

III. ANALYSIS

A. Preliminary remarks

We seek a solution of the boundary value problem (14)–(19) for small ε that varies on a scale of 2π in the circumferential direction θ. Note that the second and third terms on the left-hand side of Eq. (14) are multiplied by ε; hereinafter, we shall call the third term $-\varepsilon(1 + \varepsilon y)^{-1}\zeta_\rho \sin\theta_\zeta \, \partial\hat{f}/\partial\theta_\zeta$, which is peculiar to a curvilinear coordinate system, the curvature term for short. Then, one may consider it feasible to seek a solution using a perturbation by regarding these two terms as higher-order terms. That is, we seek the solution as a power series expansion in ε:

$$\hat{f} = \hat{f}_{(0)} + \hat{f}_{(1)}\varepsilon + \cdots. \tag{21}$$

Then, the problem will be reduced to solving a sequence of boundary value problems of the Boltzmann equation with only one derivative term with $\partial\hat{f}_{(m)}/\partial y$ ($m = 0, 1, \dots$); the derivative terms with $\partial\hat{f}_{(m)}/\partial\theta$ and $\partial\hat{f}_{(m)}/\partial\theta_\zeta$ appear as the inhomogeneous terms. In Ref. [12], the solution up to $\hat{f}_{(1)}$ is studied for a general orthogonal curvilinear coordinate system, and a Reynolds-type equation is derived. The truncation error of this equation is supposed to be of $O(\varepsilon^2)$. However, we will show that the error could be larger than $O(\varepsilon^2)$ when the Knudsen number or k is so large that $\varepsilon k^2 \sim 1$. Before explaining this, we shall present some properties of the velocity distribution function in the θ_ζ-y plane.

Figure 2(a) shows the projection

$$(1 + \varepsilon y)\sin\theta_\zeta = \text{const} \tag{22}$$

of the characteristics of Eq. (14) onto, or the trajectories of collisionless molecules in, the θ_ζ-y plane. (The configuration is symmetric with respect to $\theta_\zeta = 0$, and so we shall discuss only $\theta_\zeta > 0$.) The shaded region represents the molecular trajectories arriving from the rotating outer cylinder at $y = 1$.
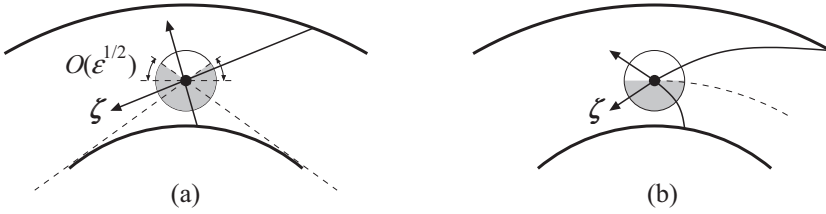
FIG. 3. Trajectories of collisionless molecules in the physical plane. (a) Trajectories corresponding to Fig. 2(a) and (b) trajectories corresponding to Fig. 2(b). Shaded area represents the range of directions of the molecular velocities arriving from the outer cylinder. In panel (b), trajectories are given by the curves (23).

The unshaded region represents those from the inner cylinder at rest at $y = 0$. Between these two regions, the velocity distribution function is discontinuous, which is a reflection of an insufficient number of intermolecular collisions. The discontinuity decays on a scale of k (or ℓ in dimensional space) in the direction tangential to the inner cylinder, which corresponds to the distance $y \sim \varepsilon k^2$ (or $r - r_1 \sim \ell^2/r_1$) from the inner cylinder [3]. Although the distribution functions in the two regions are completely different, they do not relax each other where the discontinuity is present, to result in a highly nonequilibrium region. When $\varepsilon k^2 \ll 1$, this nonequilibrium region shrinks to form a kinetic boundary layer referred to as the S layer [3,19,20]. When $\varepsilon k^2 = O(1)$, on the other hand, this nonequilibrium region covers the whole gas region. We are interested in the latter case.

Keeping this picture in mind, let us discuss the validity of the assumption that the curvature term can be regarded as a higher-order term. Suppose that $\varepsilon k^2 = O(1)$. In the θ_ζ-y plane, this assumption means that the characteristics or trajectories can be approximated by straight lines as shown in Fig. 2(b). The most significant difference from Fig. 2(a) is that the portion of the shaded region extending into $\theta_\zeta < \pi/2$ is absent. Because the distribution functions in the shaded and unshaded regions are quite different, this approximation causes an error proportional to the area of the extended portion. What should be emphasized here is that when $\varepsilon k^2 \sim 1$, the width $[O(\varepsilon k)]$ of the extended portion is of $O(\varepsilon^{1/2})$, which is much larger than ε. Therefore, even though ε is small, treating the curvature term as a higher-order term may cause a non-negligible error of $O(\varepsilon^{1/2})$ when the Knudsen number is so large that $\varepsilon k^2 \sim 1$. For example, the macroscopic flow velocity is evaluated as less in magnitude. Obviously, this is a noncontinuum effect of small curvature resulting from the finiteness of the mean-free path. Therefore, it is not surprising that a similar effect has never been discussed in continuum lubrication theory. Incidentally, one can easily see that the curvature term cannot be regarded as a higher-order term in a neighborhood $|\theta_\zeta - \pi/2| = O(\varepsilon)$, because the factor $\cos\theta_\zeta$ in the first term is as small as ε. However, the situation is more serious because the range of matter in θ_ζ is not $|\theta_\zeta - \pi/2| = O(\varepsilon)$ but much wider $|\theta_\zeta - \pi/2| = O(\varepsilon^{1/2})$, as can be seen in Fig. 2(a).

It may be instructive to restate the above discussion in the (dimensionless) physical plane. Figure 3(a) shows the molecular trajectories in Fig. 2(a) in the physical plane, which are of course straight. The shaded area represents the range of directions of molecular velocities arriving from the outer cylinder. Note that this range is wider than π because the outer cylinder is seen more widely than the inner cylinder. By an elementary manipulation, the additional angle is of $O(\varepsilon^{1/2})$. Obviously, this corresponds to the extended portion in Fig. 2(a). On the other hand, Fig. 3(b) shows the approximated trajectories in Fig. 2(b) in the physical plane. Because the Boltzmann equation is approximated, these trajectories are no longer straight, but instead are the logarithmic spirals

$$\cot\theta_\zeta \cdot \theta - \ln\hat{r} = \text{const.} \tag{23}$$

Equation (23) gives $\hat{r} = \text{constant}$ when $\theta_\zeta = \pi/2$, and the range of trajectories arriving from the outer cylinder is exactly $|\theta_\zeta| > \pi/2$ [see Fig. 2(b)]. The contribution of molecules whose velocities lie in the direction of $O(\varepsilon^{1/2})$ is incorrectly counted. Consequently, the contribution from the outer

cylinder, namely, the motion of the wall, is less evaluated. To summarize, if the curvature term is regarded as a higher-order term, then this ignores the effects caused by the fact that the number of molecules arriving from the outer cylinder is greater than that from the inner cylinder by an amount proportional to $\varepsilon^{1/2}$ owing to the curvature of the latter.

In addition to the above discussion, another effect of small curvature should also be mentioned. Consider a molecular velocity at a given point and its trace-back trajectory as shown in Fig. 3(a). The molecules arriving at this point are those departing from the portion of the boundary seen from this point. In other words, the velocity distribution function at this point is directly affected only by this visible portion of the boundary. By contrast, for the approximated Boltzmann equation represented in Fig. 3(b), the curved trajectory can arrive also from the invisible portion of the boundary. This difference is decisive when a large pressure variation is present along the channel and thus $\hat{\sigma}_a$ and $\hat{\sigma}_b$ in the boundary conditions (15) and (16) differ considerably on the invisible portion of the boundary. This is the case in the present paper; a finite pressure variation is induced by the rotation of the cylinder owing to the nonuniform accommodation coefficient, as we will see in Sec. V. The effect of small curvature here is similar to that of a weak external force on a plane Poiseuille flow of a highly rarefied gas [21].

From the above discussion, it can be seen that the solution in Ref. [12] may cause a non-negligible error even for small ε when k is sufficiently large. This will be demonstrated in Sec. V. This causes difficulties for practical applications to micro engineering. To improve the existing theory, it is natural to proceed to a higher order analysis. However, it is doubtful whether the error of $O(\varepsilon^{1/2})$ could be fixed by such an analysis. In this paper, in view of the above discussion, we try to develop an improved lubrication model for small ε that is valid even when the Knudsen number is large.

B. Plan of analysis

The discussion in Sec. III A suggests that the key to improving the theory may lie in obtaining a more precise description of the characteristic of Eq. (14). To apply the slowly varying approximation, it is necessary to distinguish the importance between the second and third terms on the left-hand side of Eq. (14). Namely, the second term is regarded as a higher-order term following the standard slowly varying approximation, whereas the third term is treated together with the first term. Specifically, we write

$$\mathcal{D}_\varepsilon = \cos\theta_\zeta \frac{\partial}{\partial y} - \frac{\varepsilon\sin\theta_\zeta}{1+\varepsilon y}\frac{\partial}{\partial\theta_\zeta}. \tag{24}$$

The $\mathcal{D}_\varepsilon$ means the derivative along Eq. (22) or the curves in Fig. 2(a). This treatment is necessary because the discontinuity in the velocity distribution function develops in the gas region and thus the individual derivatives $\partial/\partial y$ and $\partial/\partial\theta_\zeta$ are meaningless there; the sum $\cos\theta_\zeta\partial/\partial y - \varepsilon(1+\varepsilon y)^{-1}\sin\theta_\zeta\partial/\partial\theta_\zeta$ is certainly meaningful. In terms of $\mathcal{D}_\varepsilon$, the Boltzmann equation is written as

$$\zeta_\rho\mathcal{D}_\varepsilon\hat{f} + \varepsilon\frac{\zeta_\rho\sin\theta_\zeta}{1+\varepsilon y}\frac{\partial\hat{f}}{\partial\theta} = \frac{1}{k}\hat{J}(\hat{f},\hat{f}). \tag{25}$$

The solution is sought in the form of the power series expansion (21). Here $\mathcal{D}_\varepsilon$ is not expanded in ε but treated as a whole. Namely, we assume

$$\mathcal{D}_\varepsilon\hat{f} = \mathcal{D}_\varepsilon\hat{f}_{(0)} + \mathcal{D}_\varepsilon\hat{f}_{(1)}\varepsilon + \cdots, \quad \mathcal{D}_\varepsilon\hat{f}_{(m)} \sim \hat{f}_{(m)} \ (m = 0, 1, \dots). \tag{26}$$

In this way, the characteristic (22) is precisely described. Substituting Eqs. (21) and (26) into Eqs. (25) and (15)–(19) and arranging terms of the same order in ε, we obtain a sequence of boundary value problems for the spatially one-dimensional Boltzmann equations as follows. Note that the assumption (26) may fail in a neighborhood $|\theta_\zeta \pm \pi/2| = O(\varepsilon)$, in which $\mathcal{D}_\varepsilon\hat{f}_{(m)} \sim \varepsilon\hat{f}_{(m)}$ is expected. We therefore check the validity of the assumption *a posteriori* from the numerical solution in Sec. V.

C. Leading- and first-order solutions

The boundary value problem for the leading-order solution $\hat{f}_{(0)}$ is given by

$$\zeta_\rho \mathcal{D}_\varepsilon \hat{f}_{(0)} = \frac{1}{k} \hat{J}(\hat{f}_{(0)}, \hat{f}_{(0)}), \tag{27}$$

$$\hat{f}_{(0)} = [1 - \alpha_a(\theta)]\hat{f}_{(0)}(\tilde{\theta}_\zeta) + \alpha_a(\theta)\hat{\sigma}_{a(0)}E \quad (y = 0, \cos\theta_\zeta > 0), \tag{28}$$

$$\hat{f}_{(0)} = \hat{\sigma}_{b(0)}E \quad (y = 1, \cos\theta_\zeta < 0), \tag{29}$$

$$\hat{\sigma}_{a(0)} = -2\sqrt{\pi} \iiint_{\cos\theta_\zeta < 0} \zeta_\rho^2 \cos\theta_\zeta \hat{f}_{(0)} \, d\zeta_\rho \, d\theta_\zeta \, d\zeta_z \quad (y = 0),$$

$$\hat{\sigma}_{b(0)} = 2\sqrt{\pi} \iiint_{\cos\theta_\zeta > 0} \zeta_\rho^2 \cos\theta_\zeta \hat{f}_{(0)} \, d\zeta_\rho \, d\theta_\zeta \, d\zeta_z \quad (y = 1),$$

$$\int_0^{2\pi} d\theta \int_0^1 dy \iiint \zeta_\rho \hat{f}_{(0)} \, d\zeta_\rho \, d\theta_\zeta \, d\zeta_z = 2\pi. \tag{30}$$

The boundary value problem (27)–(29) can be solved independently at each θ, because the term $\partial \hat{f}_{(0)}/\partial\theta$ is not involved. The problem at a given θ is of the same form as that of a gas between coaxial cylinders at rest in which the accommodation coefficient of the inner cylinder is $\alpha_a(\theta)$. Obviously, a solution is an equilibrium state at rest:

$$\hat{f}_{(0)} = CE, \tag{31}$$

where C may be an arbitrary function of θ as long as Eq. (30) is satisfied. It will be convenient to relate C to a macroscopic variable. To do so, on substituting the expansion (21) into Eqs. (20a)–(20e), we have the following expansion of the macroscopic variables:

$$\hat{h} = \hat{h}_{(0)} + \hat{h}_{(1)}\varepsilon + \cdots, \tag{32}$$

where $\hat{h}$ stands for $\hat{\rho}$, $\hat{v}_r$, and so on. At the leading order, we have from Eq. (31) that

$$\hat{\rho}_{(0)} = \iiint \zeta_\rho \hat{f}_{(0)} \, d\zeta_\rho \, d\theta_\zeta \, d\zeta_z = C, \tag{33}$$

$$\hat{v}_{r(0)} = \frac{1}{\hat{\rho}_{(0)}} \iiint \zeta_\rho^2 \cos\theta_\zeta \hat{f}_{(0)} \, d\zeta_\rho \, d\theta_\zeta \, d\zeta_z = 0, \tag{34}$$

$$\hat{v}_{\theta(0)} = \frac{1}{\hat{\rho}_{(0)}} \iiint \zeta_\rho^2 \sin\theta_\zeta \hat{f}_{(0)} \, d\zeta_\rho \, d\theta_\zeta \, d\zeta_z = 0, \tag{35}$$

$$\hat{T}_{(0)} = \frac{2}{3\hat{\rho}_{(0)}} \iiint \zeta_\rho(\zeta_\rho^2 + \zeta_z^2)\hat{f}_{(0)} \, d\zeta_\rho \, d\theta_\zeta \, d\zeta_z = 1, \tag{36}$$

$$\hat{p}_{(0)} = \hat{\rho}_{(0)}\hat{T}_{(0)} = C. \tag{37}$$

Thus, C can be identified with the leading-order pressure $\hat{p}_{(0)}$, and we henceforth use $\hat{p}_{(0)}$ for C.

The boundary value problem for the first-order solution $\hat{f}_{(1)}$ is a linear and inhomogeneous one given by

$$\zeta_\rho \mathcal{D}_\varepsilon \hat{f}_{(1)} = \frac{2}{k} \hat{J}(\hat{f}_{(0)}, \hat{f}_{(1)}) - \zeta_\rho \sin\theta_\zeta \frac{\partial \hat{f}_{(0)}}{\partial\theta}, \tag{38}$$

$$\hat{f}_{(1)} = (1 - \alpha_a)\hat{f}_{(1)}(\tilde{\theta}_\zeta) + \alpha_a\hat{\sigma}_{a(1)}E \quad (y = 0, \cos\theta_\zeta > 0), \tag{39}$$

$$\hat{f}_{(1)} = (\hat{\sigma}_{b(1)} + 2u_w\hat{\sigma}_{b(0)}\zeta_\rho \sin\theta_\zeta)E \quad (y = 1, \cos\theta_\zeta < 0), \tag{40}$$

$$\hat{\sigma}_{a(1)} = -2\sqrt{\pi} \iiint_{\cos\theta_\zeta < 0} \zeta_\rho^2 \cos\theta_\zeta \hat{f}_{(1)} \, d\zeta_\rho \, d\theta_\zeta \, d\zeta_z \quad (y = 0),$$

$$\hat{\sigma}_{b(1)} = 2\sqrt{\pi} \iiint_{\cos\theta_\zeta > 0} \zeta_\rho^2 \cos\theta_\zeta \hat{f}_{(1)} \, d\zeta_\rho \, d\theta_\zeta \, d\zeta_z \quad (y = 1),$$

$$\int_0^{2\pi} d\theta \int_0^1 dy \iiint \zeta_\rho \hat{f}_{(1)} \, d\zeta_\rho \, d\theta_\zeta \, d\zeta_z = 0, \tag{41}$$

where $\alpha_a = \alpha_a(\theta)$. Because of the form of the inhomogeneous term and the boundary conditions, we can consistently seek the solution $\hat{f}_{(1)}$ that is odd with respect to θ_ζ. Then $\hat{\sigma}_{a(1)}$ and $\hat{\sigma}_{b(1)}$ vanish, and the subsidiary condition (41) is automatically satisfied. We further put

$$\hat{f}_{(1)} = \hat{f}_{(0)}\phi. \tag{42}$$

Substituting Eqs. (31) and (42) into Eqs. (38)–(41), we obtain a simpler problem for ϕ as

$$\zeta_\rho \mathcal{D}_\varepsilon \phi = \frac{\hat{p}_{(0)}}{k} \mathcal{L}(\phi) - \zeta_\rho \sin\theta_\zeta \frac{1}{\hat{p}_{(0)}} \frac{d\hat{p}_{(0)}}{d\theta}, \tag{43}$$

$$\phi = (1 - \alpha_a)\phi(\tilde{\theta}_\zeta) \quad (y = 0, \cos\theta_\zeta > 0), \tag{44}$$

$$\phi = 2u_w \zeta_\rho \sin\theta_\zeta \quad (y = 1, \cos\theta_\zeta < 0), \tag{45}$$

where $\mathcal{L}(\cdot)$ is the linearized collision operator defined by $E\mathcal{L}(\phi) = 2\hat{J}(E, E\phi)$. Because of the linearity, the solution is given by

$$\phi(y, \theta, \boldsymbol{\zeta}) = \frac{1}{\hat{p}_{(0)}} \frac{d\hat{p}_{(0)}}{d\theta} \Phi_{\mathrm{P}\varepsilon}\left(y, \boldsymbol{\zeta}; \frac{k}{\hat{p}_{(0)}}, \alpha_a(\theta)\right) + u_w \Phi_{\mathrm{C}\varepsilon}\left(y, \boldsymbol{\zeta}; \frac{k}{\hat{p}_{(0)}}, \alpha_a(\theta)\right), \tag{46}$$

where $\boldsymbol{\zeta}$ is the abbreviation for $(\zeta_\rho, \theta_\zeta, \zeta_z)$. The functions $\Phi_{\mathrm{P}\varepsilon}(y, \boldsymbol{\zeta}; \tilde{k}, \alpha)$ and $\Phi_{\mathrm{C}\varepsilon}(y, \boldsymbol{\zeta}; \tilde{k}, \alpha)$ are defined by Eqs. (A1)–(A3) and Eqs. (A4)–(A6), respectively, in Appendix A; the $\tilde{k}$ and α are the parameters that stand for $k/\hat{p}_{(0)}$ and $\alpha_a(\theta)$, respectively.

Substituting Eqs. (31) and (42) into Eq. (21), the solution up to $\hat{f} = \hat{f}_{(0)} + \hat{f}_{(1)}\varepsilon$ is written as

$$\hat{f}(y, \theta, \boldsymbol{\zeta}) = \hat{p}_{(0)} E \left\{ 1 + \varepsilon \left[\frac{1}{\hat{p}_{(0)}} \frac{d\hat{p}_{(0)}}{d\theta} \Phi_{\mathrm{P}\varepsilon}\left(y, \boldsymbol{\zeta}; \frac{k}{\hat{p}_{(0)}}, \alpha_a(\theta)\right) + u_w \Phi_{\mathrm{C}\varepsilon}\left(y, \boldsymbol{\zeta}; \frac{k}{\hat{p}_{(0)}}, \alpha_a(\theta)\right) \right] \right\}, \tag{47}$$

in terms of the undetermined function $\hat{p}_{(0)}(\theta)$.

D. Lubrication model

Our final task is to determine the unknown function $\hat{p}_{(0)}$, which is accomplished by using the mass conservation law. Multiplying the Boltzmann equation (14) by ζ_ρ, integrating with respect to ζ_ρ, θ_ζ, and ζ_z and with respect to y from 0 to 1, and applying the boundary condition (15) or (16), we obtain the mass conservation law $d\hat{M}/d\theta = 0$. Here $\rho_0(2RT_0)^{1/2}D\hat{M}$ is the mass flow rate of the gas per unit time and per unit depth in z, and $\hat{M} = \int_0^1 dy \iiint \zeta_\rho^2 \sin\theta_\zeta \hat{f} \, d\zeta_\rho \, d\theta_\zeta \, d\zeta_z$. Substituting Eq. (47) into the mass conservation law, we obtain

$$\frac{d}{d\theta} \left[m_{\mathrm{P}\varepsilon}\left(\frac{k}{\hat{p}_{(0)}}, \alpha_a(\theta)\right) \frac{d\hat{p}_{(0)}}{d\theta} + u_w \hat{p}_{(0)} m_{\mathrm{C}\varepsilon}\left(\frac{k}{\hat{p}_{(0)}}, \alpha_a(\theta)\right) \right] = 0, \tag{48}$$

where the functions $m_{\mathrm{P}\varepsilon}(\tilde{k}, \alpha)$ and $m_{\mathrm{C}\varepsilon}(\tilde{k}, \alpha)$ are defined by Eq. (A10) in Appendix A. As we are about to see, Eq. (48) plays a role of determining the leading-order pressure $\hat{p}_{(0)}$.

Suppose that the boundary value problem (A1)–(A3) for $\Phi_{P\varepsilon}$ and that (A4)–(A6) for $\Phi_{C\varepsilon}$ are solved for a wide range of the parameters $\tilde{k}$, α, and ε, and that the database of the functions $m_{P\varepsilon}(\tilde{k}, \alpha)$ and $m_{C\varepsilon}(\tilde{k}, \alpha)$ is known. Then Eq. (48) becomes an ordinary differential equation to determine $\hat{p}_{(0)}$. Once $\hat{p}_{(0)}$ is known, the velocity distribution function is given by Eq. (47). Substituting Eq. (47) into Eqs. (20a)–(20h), the macroscopic variables are obtained. For example, the component $\hat{v}_\theta$ of the flow velocity and those of the stress tensor up to the first order are given by

$$\hat{v}_\theta = \varepsilon \left[\frac{1}{\hat{p}_{(0)}} \frac{d\hat{p}_{(0)}}{d\theta} u_{P\varepsilon}\left(y; \frac{k}{\hat{p}_{(0)}}, \alpha_a(\theta) \right) + u_w u_{C\varepsilon}\left(y; \frac{k}{\hat{p}_{(0)}}, \alpha_a(\theta) \right) \right], \tag{49}$$

$$\hat{p}_{rr} = \hat{p}_{\theta\theta} = \hat{p} = \hat{p}_{(0)}, \tag{50}$$

$$\hat{p}_{\theta r} = \varepsilon \left[\frac{d\hat{p}_{(0)}}{d\theta} S_{P\varepsilon}\left(y; \frac{k}{\hat{p}_{(0)}}, \alpha_a(\theta) \right) + u_w \hat{p}_{(0)} S_{C\varepsilon}\left(y; \frac{k}{\hat{p}_{(0)}}, \alpha_a(\theta) \right) \right], \tag{51}$$

where the functions $u_{P\varepsilon}(y; \tilde{k}, \alpha)$ and $u_{C\varepsilon}(y; \tilde{k}, \alpha)$ are defined by Eq. (A8), and the functions $S_{P\varepsilon}(y; \tilde{k}, \alpha)$ and $S_{C\varepsilon}(y; \tilde{k}, \alpha)$ are defined by Eq. (A9). In this way, Eq. (48) plays the role of determining the pressure distribution $\hat{p}_{(0)}$. Therefore, Eq. (48) is a generalization of the Reynolds equation in continuum lubrication theory. Note that the gas-film thickness, which is a constant, does not appear in Eq. (48) because the special case of coaxial annulus is considered here.

In the derivation of Eq. (48) as well as that of Eq. (47), no restriction is imposed on k. In other words, it is implicitly assumed that $k = O(1)$. To verify that Eq. (48) is valid for the whole range of k, we put $k = 1/\varepsilon^n$ ($n = 1, 2, \ldots$) and conduct a similar analysis. As a result, we obtain Eq. (48) in which $m_{P\varepsilon}(k/\hat{p}_{(0)}, \alpha_a)$ and $m_{C\varepsilon}(k/\hat{p}_{(0)}, \alpha_a)$ are replaced respectively by $m_{P\varepsilon\infty}(\alpha_a)$ and $m_{C\varepsilon\infty}(\alpha_a)$ for an arbitrary $n \geqslant 1$. Here, $m_{P\varepsilon\infty}(\alpha_a)$ and $m_{C\varepsilon\infty}(\alpha_a)$ are given by Eq. (A10) in which Eqs. (A11) and (A12), respectively, are substituted. Because the functions $m_{P\varepsilon}(\tilde{k}, \cdot)$ and $m_{C\varepsilon}(\tilde{k}, \cdot)$ tend to $m_{P\varepsilon\infty}(\cdot)$ and $m_{C\varepsilon\infty}(\cdot)$, respectively, as $\tilde{k} \to \infty$, we find that Eq. (48) still holds even in the limit $k = \infty$ by making $n \to \infty$.

E. Remarks and supplements

It is appropriate here to go back to the beginning of Sec. III A and compare Eq. (48) with the existing generalized Reynolds equation [12]. For a coaxial annulus, this is

$$\frac{d}{d\theta} \left[m_P\left(\frac{k}{\hat{p}_{(0)}}, \alpha_a(\theta) \right) \frac{d\hat{p}_{(0)}}{d\theta} + u_w \hat{p}_{(0)} m_C\left(\frac{k}{\hat{p}_{(0)}}, \alpha_a(\theta) \right) \right] = 0, \tag{52}$$

where the functions $m_P(\tilde{k}, \alpha)$ and $m_C(\tilde{k}, \alpha)$ are the mass flow rate coefficients of Poiseuille and Couette flows of a rarefied gas between plane parallel walls defined by Eq. (B11). The derivation of and supplements to Eq. (52) are summarized in Appendix B. The parameter ε is involved in Eq. (52) through $u_w = \hat{v}_w/\varepsilon$ [see Eq. (1)]. Making ε small has two effects: it makes the curvature small and it makes the dimensionless arc length $r_1\theta/D = \varepsilon^{-1}\theta$ along the inner cylinder large. The latter effect is reflected in Eq. (52), but the former is neglected. To distinguish between the two models, Eq. (52) as well as the solution in Appendix B will be called the plane lubrication model, while Eq. (48) as well as the solution in Secs. III B–III D will be called the improved lubrication model. Although Eqs. (48) and (52) are quite similar in appearance, they are different equations when $\varepsilon > 0$, which can be seen as follows. The function $m_{C\varepsilon}$, defined by Eq. (A10) using the solution $\Phi_{C\varepsilon}$, is the coefficient of the mass flow rate (through a cross section $\theta = \text{const}$) of a cylindrical Couette flow of a rarefied gas between coaxial cylinders with dimensionless curvature ε. The function $m_{P\varepsilon}$, defined by Eq. (A10) using the solution $\Phi_{P\varepsilon}$, is the mass flow rate coefficient of a flow induced by a pressure gradient along a curved channel at rest with dimensionless curvature ε; in other words, this flow is a rarefied gas version of the basic flow of Dean's problem in fluid dynamics [22]. These functions depend on the curvature parameter ε through the operator $\mathcal{D}_\varepsilon$. Consequently, Eq. (48) depends on the curvature
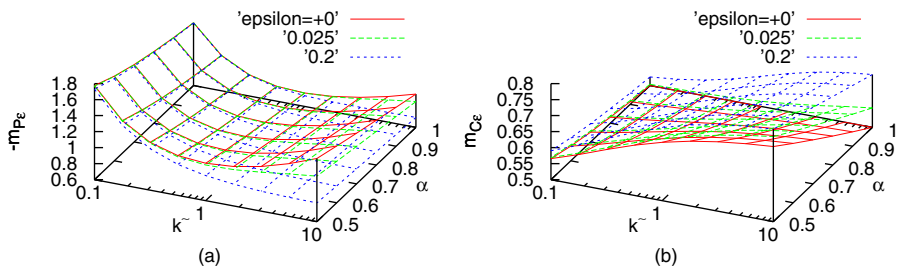
FIG. 4. Mass flow rate coefficients m_{P_ε} and m_{C_ε} as functions of $\tilde{k}$ and α (BGKW model). (a) m_{P_ε} and (b) m_{C_ε}. The surfaces are $\varepsilon = +0$ ($-m_P$), 0.025, and 0.2 from the top in (a), and $\varepsilon = +0$ (m_C), 0.025, and 0.2 from the bottom in (b).

effect, in contrast to Eq. (52). Note that m_{P_ε} and m_{C_ε} reduce to m_P and m_C, respectively, in the limit $\varepsilon = +0$, and consequently Eq. (48) coincides with Eq. (52) in this limit.

Some examples of the mass flow rate coefficients m_{P_ε} and m_{C_ε} are presented in Fig. 4. The results in this figure are computed for the BGKW kinetic model. Figure 4(a) shows the mass flow rate coefficient m_{P_ε} of the curved Poiseuille (Dean) flow as a function of the local Knudsen number $\tilde{k}$ and α. The function m_P in the plane model ($\varepsilon = +0$) is also shown for comparison. It can be seen that $-m_{P_\varepsilon}$ is a decreasing function of ε. As is well known, $-m_P$ of plane Poiseuille flow exhibits the Knudsen minimum [3] at an intermediate $\tilde{k}$ about 1. When $\varepsilon = 0.025$, $-m_{P_\varepsilon}$ also exhibits the Knudsen minimum. When $\varepsilon = 0.2$, however, the Knudsen minimum is not observed in the range $0.1 \leqslant \tilde{k} \leqslant 10$ and $0.5 \leqslant \alpha \leqslant 0.8$. From Fig. 4(a), it can be seen that there is a significant difference from the plane case m_P for large $\tilde{k}$. In fact, m_P of the plane flow diverges as $\tilde{k} \to \infty$ whereas m_{P_ε} of the curved flow remains finite at $\tilde{k} = \infty$ [see Eq. (A11)]; the velocity distribution function does not diverge because the characteristic is correct and thus the contribution of the molecules arriving from the correct range in Fig. 3(a) is counted. Figure 4(b) shows the mass flow rate m_{C_ε} of cylindrical Couette flow as well as that m_C of plane Couette flow. It can be seen that the m_{C_ε} is an increasing function of $\tilde{k}$, a decreasing function of α, and an increasing function of ε. There is a significant difference from the plane case m_C at large $\tilde{k}$. From Fig. 4, it is observed that the difference between m_{P_ε} and m_P, as well as that between m_{C_ε} and m_C, is noticeable even when ε is 0.025 and $\tilde{k}$ is about 1. Consequently, a non-negligible difference is expected between the solutions of the two lubrication models (48) and (52). A simple database of the functions m_{P_ε}, m_{C_ε}, m_P, and m_C is provided in Appendix C. It may be noted that the analysis in Sec. III is valid for a standard Boltzmann equation. Although the results in Fig. 4 and in Sec. V are presented for the BGKW model, results for an arbitrary molecular model are immediately obtained by simply replacing the linearized collision integral $\mathcal{L}(\cdot)$.

In this way, two lubrication models have been derived, namely, the plane model (52) and the improved model (48). Our interest now is in examining how well these two models approximate the true solution of the Boltzmann equation. To this end, a direct numerical analysis of the Boltzmann equation is conducted to provide a reference for an assessment of these models. The remainder of the paper is devoted to this assessment.

IV. NUMERICAL ANALYSIS

A. Supplements to the problem

For an assessment of the lubrication models in Sec. III, a direct numerical analysis of the boundary value problem (14)–(19) is conducted. In the present paper, the distribution of the

accommodation coefficient $\alpha_a(\theta)$ of the inner cylinder is given by

$$
\alpha_a(\theta) = \begin{cases} \alpha_2 & (0 \leqslant \theta/\pi < c - b), \\ \dfrac{\alpha_2 + \alpha_1}{2} - \dfrac{\alpha_2 - \alpha_1}{2} \sin \dfrac{\theta - c\pi}{2b} & (c - b \leqslant \theta/\pi < c + b), \\ \alpha_1 & (c + b \leqslant \theta/\pi \leqslant 1), \\ \alpha_a(2\pi - \theta) & (1 < \theta/\pi < 2), \end{cases} \tag{53}
$$

where α_1, α_2, b, and c are positive constants such that $0 < \alpha_1 \leqslant \alpha_2 \leqslant 1$, $0 < b \leqslant 1/2$, and $b \leqslant c \leqslant 1 - b$. The function (53) is symmetric with respect to $\theta = \pi$. The distribution (53) is adopted because it can produce a wide variation of the eccentric force (11). An example is depicted in Fig. 1(b) for $\alpha_1 = 0.5, \alpha_2 = 1, b = 0.1$, and $c = 0.5$, for which most of the computations are conducted. We employ the BGKW kinetic model for this computation. That is, the collision integral is given by

$$
\hat{J}(\hat{f}, \hat{f}) = \hat{\rho}(\hat{f}_e - \hat{f}),
$$

$$
\hat{f}_e = \frac{\hat{\rho}}{(\pi \hat{T})^{3/2}} \exp \left(-\frac{(\zeta_\rho \cos \theta_\zeta - \hat{v}_r)^2 + (\zeta_\rho \sin \theta_\zeta - \hat{v}_\theta)^2 + \zeta_z^2}{\hat{T}} \right), \tag{54}
$$

where $\hat{\rho}, \hat{v}_r, \hat{v}_\theta$, and $\hat{T}$ are given by Eqs. (20a)–(20d). For the BGKW kinetic model, incidentally, the mean-free path ℓ is related to the viscosity μ of the gas by [3]

$$
\mu = \frac{\sqrt{\pi}}{2} \frac{p_0}{(2RT_0)^{1/2}} \ell. \tag{55}
$$

The boundary value problem (14)–(19) with Eqs. (53) and (54) is characterized by the following seven dimensionless parameters

$$
\varepsilon = \frac{D}{r_1}, \quad \mathrm{Kn} = \frac{\ell}{D}, \quad \hat{v}_w = \frac{v_w}{(2RT_0)^{1/2}}, \quad \alpha_1, \quad \alpha_2, \quad b, \text{ and } c. \tag{56}
$$

In this paper, the computations are conducted only for the cases of $\hat{v}_w = 0.1, \alpha_1 = 0.5, \alpha_2 = 1$, and $b = 0.1$. The parameter c is a measure of the coverage of the diffuse reflection area ($\alpha_a = \alpha_2 = 1$) of the surface of the inner cylinder.

B. Numerical method

The method of numerical analysis adopted here is essentially the same as that used in Ref. [23]. Therefore, it is outlined only briefly.

First, the following marginal distribution functions are introduced [24]:

$$
g_1 = \int_{-\infty}^{\infty} \hat{f} \, d\zeta_z, \quad g_2 = 2 \int_{-\infty}^{\infty} \zeta_z^2 \hat{f} \, d\zeta_z. \tag{57}
$$

Then, the boundary value problem (14)–(19) for the five independent variables $y, \theta, \zeta_\rho, \theta_\zeta$, and ζ_z is reduced to a simultaneous problem for g_1 and g_2 for the four independent variables y, θ, ζ_ρ, and θ_ζ. The infinite range $0 \leqslant \zeta_\rho < \infty$ is replaced by a finite range $0 \leqslant \zeta_\rho \leqslant \zeta_D$, where ζ_D is a constant to be given in Sec. IV B. The Boltzmann equation and the boundary conditions are solved numerically in the four-dimensional finite domain $0 \leqslant y \leqslant 1, 0 \leqslant \theta \leqslant 2\pi, 0 \leqslant \zeta_\rho \leqslant \zeta_D$, and $-\pi \leqslant \theta_\zeta \leqslant \pi$ using a finite difference method by iteration. To reduce the numerical error in the computation of the macroscopic variables (20a)–(20h) and thus the collision term (54), the numerical integration is conducted on the subtracted quantity $\hat{f} - \hat{f}_{(0)}$ rather than on $\hat{f}$ itself, which is especially efficient when Kn and ε are small.

A feature of the present problem is that the velocity distribution function is discontinuous across the surfaces

$$
(1 + \varepsilon y) \sin \theta_\zeta = \pm 1 \quad \left(|\theta_\zeta| < \frac{\pi}{2}, \, 0 \leqslant \theta \leqslant 2\pi \right) \tag{58}
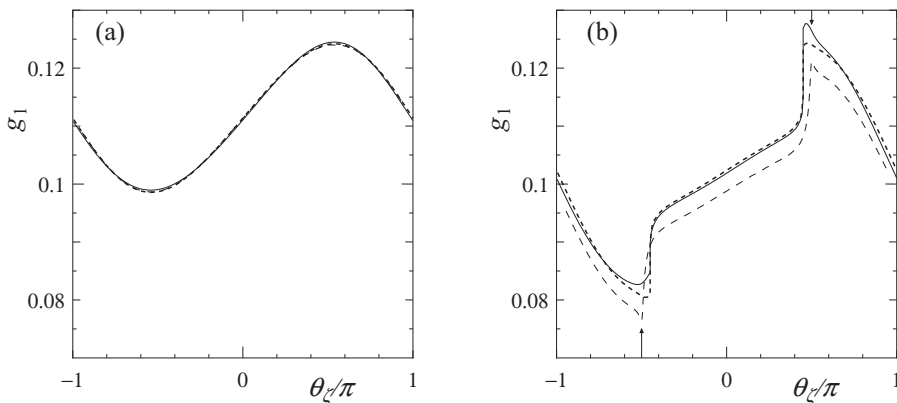$$

FIG. 5. Marginal velocity distribution function g_1 [Eq. (57)] at the cross section $y = 1/2$, $\theta = \pi/2$, and $\zeta_\rho = 1$ ($\varepsilon = 0.025$ and $c = 0.5$). (a) Kn $= 0.1$ and (b) Kn $= 10$. Solid line for the direct numerical solution; dotted line for the improved lubrication model (47); dashed line for the plane lubrication model (B4). The functions represented by the solid and the dotted lines are discontinuous at $\theta_\zeta/\pi = \pm\mathrm{Arcsin}(1 + \varepsilon y)^{-1}/\pi (= \pm0.4499)$. The vertical arrows indicate $\theta_\zeta/\pi = \pm1/2$.

in the three-dimensional space of y, θ, and θ_ζ. The finite difference method cannot be applied across the discontinuous surface. In this paper, the hybrid scheme of characteristic coordinate and finite difference methods devised in Ref. [18] is applied to bypass this difficulty.

C. Computational conditions and accuracy tests

The computational conditions are as follows. For the y coordinate, the $N_y + 1$ mesh points are arranged nonuniformly in the interval $0 \leqslant y \leqslant 1$, where $N_y = 320$. The mesh size is minimum 0.00011 at $y = 0$ and $y = 1$ and is uniform and maximum 0.005 in the interval $0.16 \leqslant y \leqslant 0.84$. For θ, $N_\theta + 1$ mesh points are arranged uniformly in the interval $0 \leqslant \theta \leqslant 2\pi$, where $N_\theta = 320$. For ζ_ρ, $N_u + 1$ mesh points are arranged uniformly in $0 \leqslant \zeta_\rho \leqslant \zeta_D$, where $N_u = 40$ and $\zeta_D = 5$. For θ_ζ, $N_v + 1$ mesh points are arranged uniformly in the interval $-\pi \leqslant \theta_\zeta \leqslant \pi$, where $N_v = 640$.

For a test of accuracy of the numerical solution, we conducted recomputations using coarser mesh systems in addition to the production run P with $(N_y, N_\theta, N_u, N_v) = (320, 40, 320, 640)$, namely, the coarser system A with $(N_y, N_\theta, N_u, N_v) = (160, 30, 160, 320)$ and the coarsest system B with $(N_y, N_\theta, N_u, N_v) = (80, 22, 80, 160)$. By examining the differences between the three runs, i.e., B–P and A–P, the error in the production run P is estimated. From this test, it is estimated that the numerical error in the dimensionless pressure $\hat{p}$ over $0 \leqslant \theta \leqslant 2\pi$ at $y = 0$ is less than 0.03%, and that the numerical error in the flow velocity $\hat{v}_\theta$ over $0 \leqslant y \leqslant 1$ at the cross section $\theta = 0$ is less than 0.04%. Further, the numerical errors in the eccentric force (F_1, F_2) [Eq. (11)] and the torque N [Eq. (12)] are estimated to be less than 0.11% over the range of $0.1 \leqslant$ Kn $\leqslant 10$, $0.025 \leqslant \varepsilon \leqslant 0.2$, and $c = 0.5$. Especially at Kn $= 1$ and $c = 0.5$, the error in the eccentric force is less than 0.04% over $0.025 \leqslant \varepsilon \leqslant 0.2$.

V. RESULTS

A. Velocity distribution function

We first present a few examples of the velocity distribution function. In Fig. 5 the marginal distribution function g_1 [Eq. (57)] at the cross section $y = 1/2$, $\theta = \pi/2$, and $\zeta_\rho = 1$ is presented as a function of θ_ζ. The solid line represents the solution of the direct numerical analysis of Eqs. (14)–(19), the dotted line represents the solution (47) of the improved lubrication model, and the dashed line represents the solution (B4) of the plane lubrication model. When the Knudsen number is small
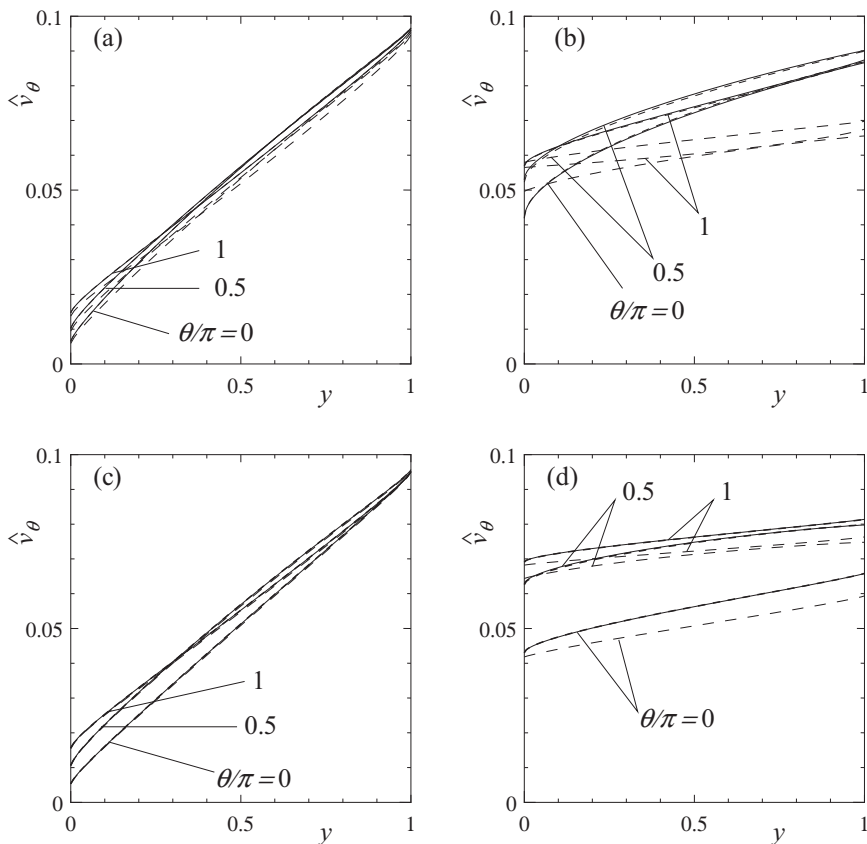
FIG. 6. Profile of the dimensionless flow velocity $\hat{v}_\theta$ ($c = 0.5$). (a) (ε, Kn)=(0.2, 0.1), (b) (0.2, 10), (c) (0.025, 0.1), and (d) (0.025, 10). Solid line for the direct numerical solution; dotted line for the improved lubrication model (49); dashed line for the plane lubrication model (B12).

[Fig. 5(a)], the results of the both lubrication models agree satisfactorily with the direct numerical solution. When the Knudsen number is large [Fig. 5(b)], however, some disagreement is observed. We first survey the behavior of the distribution function on the basis of the direct numerical solution (solid line); we consider only the half interval $\theta_\zeta > 0$ for simplicity. The distribution function consists of two portions: one portion $\theta_\zeta > \mathrm{Arcsin}(1 + \varepsilon y)^{-1} (= 0.4499\pi)$ for the molecules directly arriving from the outer cylinder, and the other $\theta_\zeta < \mathrm{Arcsin}(1 + \varepsilon y)^{-1}$ for those from the inner cylinder. The distribution function is discontinuous at their boundary $\theta_\zeta = \mathrm{Arcsin}(1 + \varepsilon y)^{-1}$, at which the solid line is vertical. Note that the former portion extends to $\theta_\zeta = \mathrm{Arcsin}(1 + \varepsilon y)^{-1}$ beyond $\theta_\zeta = \pi/2$, which corresponds to the extended area in Fig. 2(a). The distribution function of the plane model (dashed line) abruptly changes around $\theta_\zeta = \pi/2$. Therefore, the behavior of the plane model is incorrect in the interval $\mathrm{Arcsin}(1 + \varepsilon y)^{-1}(= 0.4499\pi) < \theta_\zeta < \pi/2$, which is noticeable in the figure. By contrast, the result of the improved lubrication model (dotted line) certainly describes the position of the discontinuity correctly, and the distribution function agrees with the solid line fairly well. The disagreement is most significant around $\theta_\zeta/\pi = 1/2$. This disagreement may be attributed to the inconsistency of the assumption (26) in a neighborhood of $\theta_\zeta = \pi/2$. It is, however, localized, and its magnitude is approximately 0.004, which is of the order of the truncation error $\hat{f}_{(0)}\hat{v}_w^2 \simeq 0.1 \times 0.1^2 = 0.001$ of the perturbation. Therefore, the inconsistency of our assumption around $\theta_\zeta = \pi/2$ does not seem to produce a serious error.
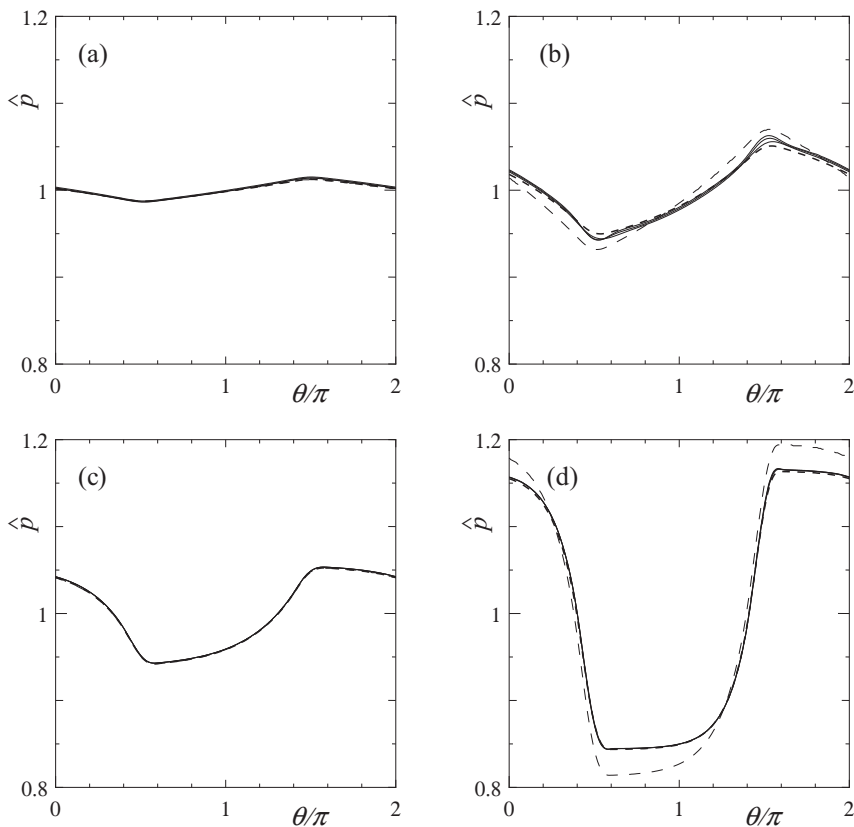
FIG. 7. Distribution of the dimensionless pressure $\hat{p}$ along the channel ($c = 0.5$). (a) (ε, Kn) = (0.2, 0.1), (b) (0.2, 10), (c) (0.025, 0.1), and (d) (0.025, 10). For the key, see the caption of Fig. 6.

B. Macroscopic variables

The profiles of the flow velocity $\hat{v}_\theta$ at the three cross sections $\theta/\pi = 0, 0.5$, and 1 are presented in Fig. 6. The values of the accommodation coefficient α_a of the inner cylinder at these cross sections are 1, 0.75, and 0.5, respectively. The meaning of the lines is the same as in Fig. 5. We first survey the flow behavior on the basis of the direct numerical solution (solid line). When the Knudsen number is small [Figs. 6(a) and 6(c)], the velocity profile depends only weakly on the position θ of the cross section. This is easily understood that when the Knudsen number is small, the velocity slip on the cylinders is small, regardless of the distribution of the accommodation coefficient, and thus the flow is disturbed only slightly from the axisymmetric flow. When the Knudsen number is large [Figs. 6(b) and 6(d)], the velocity profile shows a clear dependence on the cross section. The velocity profile at $\theta = 0$ is smallest at which the accommodation coefficient is maximum. Now let us compare the results of the two lubrication models. When the Knudsen number is small [Figs. 6(a) and 6(c)], the results of the both lubrication models agree with the direct numerical solution very well. When the Knudsen number is large [Figs. 6(b) and 6(d)], a considerable difference is observed between the plane model (dashed line) and the direct numerical solution (solid line). By contrast, the improved model (dotted line) agrees with the direct numerical solution very well. Note that the flow velocity $\hat{v}_\theta$ of the plane model (dashed line) is smaller than that of the direct numerical solution in the bulk region, in agreement with the estimate in Sec. III A.

Next, the pressure distribution $\hat{p}$ along the channel is presented in Fig. 7. Figures 7(a)–7(d) are for the same cases as those in Figs. 6(a)–6(d), respectively. For the direct numerical solution (solid
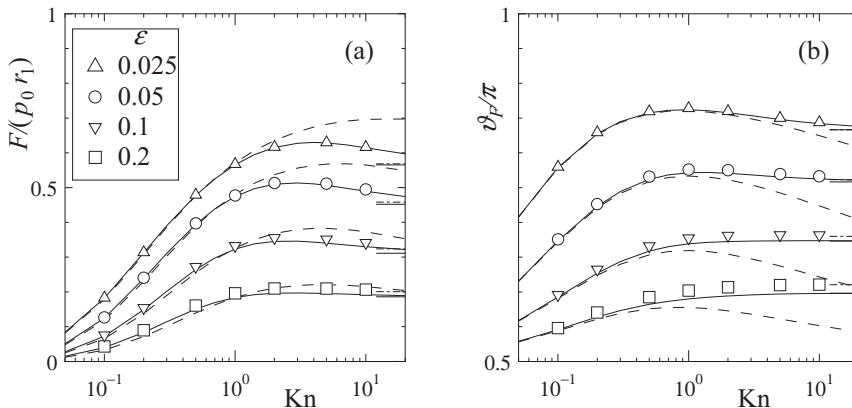
FIG. 8. Magnitude F and the direction ϑ_F [Eq. (59)] of the eccentric force [Eq. (11)] as functions of Kn and ε ($c = 0.5$). (a) Magnitude F and (b) the direction ϑ_F. Symbols for the direct numerical solution; triangle ($\triangle$) for $\varepsilon = 0.025$; circle ($\bigcirc$) for $\varepsilon = 0.05$; downtriangle ($\triangledown$) for $\varepsilon = 0.1$; square ($\square$) for $\varepsilon = 0.2$. Solid line for the improved lubrication model; dashed line for the plane lubrication model. Horizontal lines are the asymptotes for Kn $= \infty$; dot-dashed line for the direct numerical solution; solid line for the improved lubrication model. The lines are for $\varepsilon = 0.025, 0.05, 0.1$, and 0.2 from the top. In panel (b), two asymptotes are indistinguishable at $\varepsilon = 0.025$ and 0.05.

line), the pressure distributions are plotted along the three lines $y = 0, 0.5$, and 1; they are almost indistinguishable in agreement with the analytical solution (31). Figures 7(a) and 7(b) are for cases of relatively large ε. When the Knudsen number is small [Fig. 7(a)], the pressure variation is small, which is expected from Fig. 6(a) because the flow is nearly axisymmetric. When the Knudsen number is large [Fig. 7(b)], a finite pressure variation is induced owing to an acceleration and a deceleration along the channel shown in Fig. 6(b). Figures 7(c) and 7(d) are for cases of smaller $\varepsilon(= 0.025)$. The pressure variation is larger than that for $\varepsilon = 0.2$. This is because the circumferential length of the channel $2\pi r_1 = 2\pi D/\varepsilon$ is inversely proportional to ε, and so the pressure gradient accumulates over a long length for a small ε. Moreover, when Kn $= 10$ [Fig. 7(d)], the pressure distribution splits into a high-pressure region about $\theta = 0$ and a low-pressure region about $\theta = \pi$. This pressure difference contributes to the eccentric force to be discussed in Sec. V C. Now let us compare the results of the two lubrication models with the direct numerical solution. When the Knudsen number is small [Figs. 7(a) and 7(c)], both models agree very well with the direct numerical solution. When the Knudsen number is large [Figs. 7(b) and 7(d)], a non-negligible disagreement is observed in the plane model (dashed line). By contrast, the improved model (dotted line) shows a good agreement. Incidentally, when the pressure variation is so small that the problem may be linearized, the pressure variation $\hat{p} - 1$ is antisymmetric with respect to $\theta = \pi$ provided that the accommodation coefficient α_a is symmetric with respect to $\theta = \pi$ [23]. This tendency is observed in Fig. 7(a). The breaking of the antisymmetry seen in Figs. 7(b)–7(d) is therefore due to the nonlinear effect of the finite pressure variation.

C. Eccentric force and torque

Let the magnitude F and the direction ϑ_F of the eccentric force (F_1, F_2) [Eq. (11)] acting on the inner cylinder be defined by

$$F_1 = F \cos \vartheta_F, \quad F_2 = F \sin \vartheta_F. \tag{59}$$

They are presented in Figs. 8(a) and 8(b), respectively, as functions of the Knudsen number Kn and the dimensionless curvature ε. The symbols represent the direct numerical solution, the solid
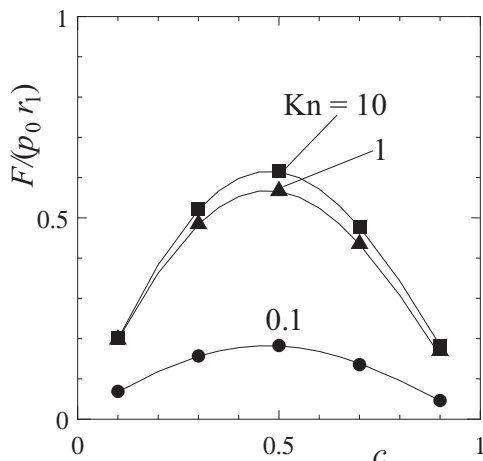
FIG. 9. Magnitude F [Eq. (59)] of the eccentric force as a function of c ($\varepsilon = 0.025$). Markers for the direct numerical solution; circle ($\bullet$) for Kn = 0.1; triangle ($\blacktriangle$) for Kn = 1; square ($\blacksquare$) for Kn = 10. Solid line for the improved lubrication model; the lines are for Kn = 0.1, 1, and 10 from the bottom.

line represents the result of the improved lubrication model, and the dashed line represents that of the plane lubrication model. When the problem can be linearized [23], the magnitude F is an increasing function of Kn, and the direction is $\vartheta_F = \pi/2$ (i.e., $F_1 = 0$) regardless of the parameters (56). The force due to the pressure difference seen in Fig. 7(d) acts in the $\theta = \pi$ direction and becomes stronger as ε decreases. Consequently, the magnitude F increases and the direction ϑ_F approaches π. For sufficiently small ε, the magnitude F takes its maximum value at an intermediate Knudsen number. Similar behavior is observed also in the direction ϑ_F in Fig. 8(b). Now let us examine the performance of the two lubrication models. When the Knudsen number is small, both models agree very well with the direct numerical solution. For example, at Kn = 1 and $\varepsilon = 0.05$ (i.e., $\varepsilon \text{Kn}^2 = 0.05$), the error in F of the plane lubrication model (dashed line) compared with the direct numerical solution (symbols) is 0.6% ($= 6 \times 10^{-3}$), which is certainly of the order of $\varepsilon^2 (= 2.5 \times 10^{-3})$. As the Knudsen number increases, however, a non-negligible disagreement appears in the plane lubrication model. The disagreement is noticeable even when $\varepsilon = 0.025$ and Kn = 2. By contrast, the result of the improved model (solid line) agrees with the direct numerical solution over the whole range of the Knudsen number. The agreement at the smallest $\varepsilon (= 0.025)$ is excellent even in the limit of Kn = ∞.

The results up to here are those for a coverage $c = 0.5$ of the diffuse reflection area. Figure 9 presents the magnitude F of the eccentric force as a function of c. The magnitude F of the force takes its maximum value at approximately $c = 0.5$. This can easily be understood as follows. When c approaches 0 or 1, the distribution of the accommodation coefficient α_a approaches a uniform distribution $\alpha_a = \alpha_1$ or $\alpha_a = \alpha_2$, respectively. Consequently, the flow approaches an axially symmetric one, in which the eccentric force vanishes. The improved lubrication model approximates the direct numerical solution well over the whole range of c.

The torque N [Eq. (12)] acting on the inner cylinder is presented in Fig. 10 as a function of Kn and ε. The torque is an increasing function of Kn, and increases as ε decreases. The result of the improved lubrication model (solid line) agrees very well with the direct numerical solution (symbols). Note that the error of the plane lubrication model (dotted line) is much smaller than that in the eccentric force in Fig. 8. This is because the torque N is an integral of the shear stress $\hat{p}_{\theta r}$ given by the moment (20g): the effect of the extended portion about $\theta_\zeta = \pi/2$ [Fig. 2(a)], which is the main source of the error, is canceled out by the factor $\cos\theta_\zeta$ in the integrand that vanishes at $\theta_\zeta = \pi/2$.
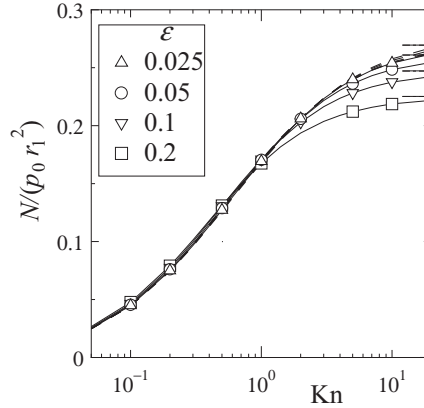
FIG. 10. Torque N [Eq. (12)] acting on the inner cylinder as a function of Kn and ε ($c = 0.5$). For the key, see the caption of Fig. 8. The asymptotes for Kn $= \infty$ of the direct numerical solution and those for the improved lubrication model are indistinguishable.

Finally, let us examine the dependence of the error of the plane lubrication model on the dimensionless curvature ε. In Fig. 8(a), it appears that the difference in the magnitude F between the plane lubrication model and the direct numerical solution increases monotonically as ε decreases. Let us focus on the relative error. In Fig. 11 the symbols represent the relative errors ΔF and ΔN of the eccentric force and of the torque, respectively, as functions of ε for the Knudsen number such that $\varepsilon \mathrm{Kn}^2 = \mathrm{const} = 2$. Here, $\Delta F = |F_{\mathrm{plane}} - F_{\mathrm{DNS}}|/F_{\mathrm{DNS}}$ is the relative error in F of the plane lubrication model F_{plane} compared with the direct numerical solution F_{DNS}; a similar notation applies to N. The relative error ΔF first increases with decreasing ε, takes its maximum value at approximately $\varepsilon = 0.05$, and then decreases. The ΔF is 0.12 (12%) when $\varepsilon = 0.025$. The relative error ΔN is much smaller, as we saw in Fig. 10. Unfortunately, the direct numerical analysis for ε smaller than 0.025 is difficult. On the other hand, we have found that the improved lubrication model approximates the direct numerical solution well for small ε. Thus, we may estimate the behavior
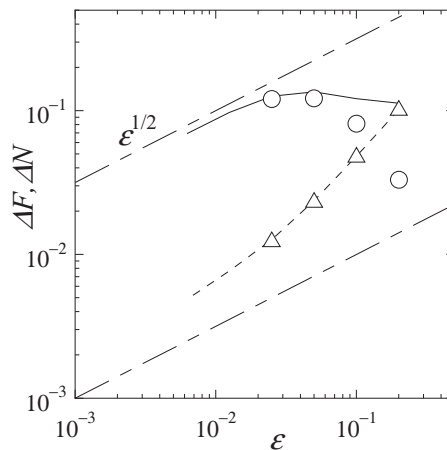
FIG. 11. Relative errors ΔF and ΔN of the plane lubrication model as functions of ε [Kn $= (2/\varepsilon)^{1/2}$, $c = 0.5$]. Circle ($\bigcirc$) and solid line for ΔF; triangle ($\triangle$) and dotted line for ΔN. Lines represent the relative errors in which the direct numerical solution is replaced by the result of the improved lubrication model; see the main text. Dash-dotted lines represent $\varepsilon^{1/2}$ and $10^{-3/2}\varepsilon^{1/2}$.

of the relative error for smaller ε by a modified ΔF in which F_{DNS} is replaced by the result F of the improved model. This result is represented by the solid (ΔF) and dotted (ΔN) lines. The lines coincide with the symbols for sufficiently small ε. This result shows that the speed of the decay is approximately $\varepsilon^{1/2}$ rather than ε^2.

From these results, we may conclude that the plane lubrication model results in a non-negligible error of $O(\varepsilon^{1/2})$ for large Knudsen numbers. We may also conclude that the improved model provides a uniformly valid approximation to the solution of the Boltzmann equation over the whole range of the Knudsen number. The success of the improved model confirms that the large error in the plane model is due to the mechanism discussed in Sec. III A. In conventional lubrication theory for a small ε, the basic equation is frequently replaced by the Reynolds equation for the vanishing curvature. We must be careful to use this substitution when a microscale lubrication at a large Knudsen number is concerned.

VI. CONCLUSION

In this paper, we studied the lubrication flow of a gas in a microscale gap between coaxial circular cylinders on the basis of kinetic theory. The stationary inner cylinder was taken to be a Maxwell-type boundary with a nonuniform accommodation coefficient in the circumferential direction, and the outer cylinder was taken to be a diffuse reflection boundary rotating at a constant speed. The dimensionless curvature ε, defined as the gap size divided by the radius of the inner cylinder, was assumed to be small, and the Knudsen number based on the gap size was arbitrary. The Boltzmann equation was studied analytically using the slowly varying approximation with special attention being paid to the characteristics of the equation. Two macroscopic lubrication models were derived: one consisting of plane Couette and Poiseuille flows (the plane lubrication model), and the other consisting of the cylindrical Couette flow and a curved Poiseuille flow (the improved lubrication model). For an assessment of the models, a direct numerical analysis of the flow was also conducted using the BGKW kinetic equation. The main results are as follows.

(1) The plane lubrication model leads to a non-negligible error of $O(\varepsilon^{1/2})$ when the Knudsen number is sufficiently large. This error is caused by neglect of the fact that the number of molecules arriving from the outer cylinder is greater than the number of those arriving from the inner cylinder by an amount proportional to $\varepsilon^{1/2}$.

(2) The improved lubrication model exhibits an excellent agreement with the direct numerical solution over the whole range of the Knudsen number.

In this paper, we have considered a simplified flow problem between coaxial circular cylinders. In practical applications, however, the lubrication effect induced by eccentricity is more important. To deal with this, an elaborate analysis using curvilinear coordinates, such as bipolar coordinates, is necessary. This analysis is a considerably cumbersome task for the Boltzmann equation. This task is left for future study.

ACKNOWLEDGMENT

APPENDIX A: FUNCTIONS RELATED TO THE LUBRICATION MODEL

The boundary value problem for $\Phi_{\text{P}\varepsilon}(y, \boldsymbol{\zeta}; \tilde{k}, \alpha)$ is

$$\zeta_\rho \mathcal{D}_\varepsilon \Phi_{\text{P}\varepsilon} - \frac{1}{\tilde{k}}\mathcal{L}(\Phi_{\text{P}\varepsilon}) = -\zeta_\rho \sin\theta_\zeta, \tag{A1}$$

$$\Phi_{\text{P}\varepsilon} = (1-\alpha)\Phi_{\text{P}\varepsilon}(\tilde{\theta}_\zeta) \quad (y=0, \cos\theta_\zeta > 0), \tag{A2}$$

$$\Phi_{\text{P}\varepsilon} = 0 \quad (y=1, \cos\theta_\zeta < 0). \tag{A3}$$

Similarly, the boundary value problem for $\Phi_{C\varepsilon}(y, \boldsymbol{\zeta}; \tilde{k}, \alpha)$ is

$$\zeta_\rho \mathcal{D}_\varepsilon \Phi_{C\varepsilon} - \frac{1}{\tilde{k}} \mathcal{L}(\Phi_{C\varepsilon}) = 0, \tag{A4}$$

$$\Phi_{C\varepsilon} = (1 - \alpha) \Phi_{C\varepsilon}(\tilde{\theta}_\zeta) \quad (y = 0, \cos\theta_\zeta > 0), \tag{A5}$$

$$\Phi_{C\varepsilon} = 2\zeta_\rho \sin\theta_\zeta \quad (y = 1, \cos\theta_\zeta < 0). \tag{A6}$$

The solutions $\Phi_{P\varepsilon}$ and $\Phi_{C\varepsilon}$ can be sought in the form $\Phi_{J\varepsilon} = \zeta_\rho \sin\theta_\zeta \Psi_J(y, \zeta_\rho, \theta_\zeta, \zeta_z)$ (J = P and C), where Ψ_J is even with respect to θ_ζ [3]. For the BGKW kinetic model used in Sec. IV, the linearized collision integral is

$$\mathcal{L}(\Phi) = \iiint K(\boldsymbol{\zeta}, \boldsymbol{\zeta}_*) \Phi(\boldsymbol{\zeta}_*) \zeta_{\rho*} E_* \, d\zeta_{\rho*} \, d\theta_{\zeta*} \, d\zeta_{z*},$$

$$K(\boldsymbol{\zeta}, \boldsymbol{\zeta}_*) = 1 + 2\zeta_\rho \zeta_{\rho*} \cos(\theta_\zeta - \theta_{\zeta*}) + 2\zeta_z \zeta_{z*} + \frac{2}{3}\left(\zeta_\rho^2 + \zeta_z^2 - \frac{3}{2}\right)\left(\zeta_{\rho*}^2 + \zeta_{z*}^2 - \frac{3}{2}\right), \tag{A7}$$

where $E_* = \pi^{-3/2} \exp(-\zeta_{\rho*}^2 - \zeta_{z*}^2)$. For Eq. (A7), Ψ_J is independent of ζ_z.

The normalized flow velocities $u_{P\varepsilon}$ and $u_{C\varepsilon}$ are defined by

$$u_{J\varepsilon}(y; \tilde{k}, \alpha) = \int \zeta_\rho^2 \sin\theta_\zeta \Phi_{J\varepsilon}(y, \boldsymbol{\zeta}; \tilde{k}, \alpha) E \, \mathbf{d\zeta} \quad (J = P \text{ and } C). \tag{A8}$$

Similarly, the normalized shear stresses $S_{P\varepsilon}$ and $S_{C\varepsilon}$ are defined by

$$S_{J\varepsilon}(y; \tilde{k}, \alpha) = 2 \int \zeta_\rho^3 \cos\theta_\zeta \sin\theta_\zeta \Phi_{J\varepsilon}(y, \boldsymbol{\zeta}; \tilde{k}, \alpha) E \, \mathbf{d\zeta} \quad (J = P \text{ and } C). \tag{A9}$$

The mass flow rate coefficients $m_{P\varepsilon}$ and $m_{C\varepsilon}$ are defined by

$$m_{J\varepsilon}(\tilde{k}, \alpha) = \int_0^1 u_{J\varepsilon}(y; \tilde{k}, \alpha) \, dy \quad (J = P \text{ and } C). \tag{A10}$$

For $\tilde{k} = \infty$, the solution $\Phi_{P\varepsilon}$ is given by

$$\Phi_{P\varepsilon}/(\hat{r} \sin\theta_\zeta) = \begin{cases} -\ln\left(\dfrac{\hat{r}(1 + \cos\theta_\zeta)}{1 + \varepsilon^{-1} - [(1 + \varepsilon^{-1})^2 - \hat{r}^2 \sin^2\theta_\zeta]^{1/2}}\right) & [|\theta_\zeta| > \text{Arcsin}\,(\varepsilon\hat{r})^{-1}], \\ -\ln\left(\dfrac{\hat{r}(1 + \cos\theta_\zeta)}{\varepsilon^{-1} + (\varepsilon^{-2} - \hat{r}^2 \sin^2\theta_\zeta)^{1/2}}\right) \\ \quad -(1 - \alpha)\ln\left(\dfrac{\varepsilon^{-1} - (\varepsilon^{-2} - \hat{r}^2 \sin^2\theta_\zeta)^{1/2}}{1 + \varepsilon^{-1} - [(1 + \varepsilon^{-1})^2 - \hat{r}^2 \sin^2\theta_\zeta]^{1/2}}\right) \\ \quad [|\theta_\zeta| < \text{Arcsin}\,(\varepsilon\hat{r})^{-1}], \end{cases} \tag{A11}$$

and the solution $\Phi_{C\varepsilon}$ is given by

$$\Phi_{C\varepsilon} = \begin{cases} 2\varepsilon(1 + \varepsilon)^{-1}\hat{r}\zeta_\rho \sin\theta_\zeta & [|\theta_\zeta| > \text{Arcsin}\,(\varepsilon\hat{r})^{-1}], \\ (1 - \alpha)2\varepsilon(1 + \varepsilon)^{-1}\hat{r}\zeta_\rho \sin\theta_\zeta & [|\theta_\zeta| < \text{Arcsin}\,(\varepsilon\hat{r})^{-1}], \end{cases} \tag{A12}$$

where $\hat{r}$ is given by Eq. (13). Note that this solution $\Phi_{P\varepsilon}$ does not diverge in contrast to the plane Poiseuille flow [3].

APPENDIX B: DERIVATION OF THE PLANE LUBRICATION MODEL

The derivation of the plane lubrication model (52) is a special case of that in Ref. [12] and quite similar to that in Secs. III B–III D, and so it is outlined only briefly.

The basic equations are Eqs. (14)–(19), that is, Eq. (25) is replaced by the original form (14) without using $\mathcal{D}_\varepsilon$. The solution $\hat{f}$ is sought in the form of the power series expansion (21), where

TABLE I. Coefficients c_{Pmn} in Eq. (C1) (BGKW model).

ε	m	$n = 0$	1	2	3	4	5	6	7	8
+0	0	−1.35453	0.34433	−0.47874	0.14753	−0.05009	0.01556	−0.00395	0.00080	−0.00011
	1	0.18233	−0.00364	0.03031	0.00433	−0.00266	0.00041	0.00021	−0.00013	0.00003
	2	0.00237	0.01456	−0.00105	0.00013	0.00036	−0.00013	−0.00001	0.00001	−0.00001
	3	0.00017	0.00021	0.00042	−0.00011	−0.00002	0.00002	0.00001	0.00001	0.00001
0.025	0	−1.28177	0.46192	−0.41206	0.17332	−0.04553	0.01421	−0.00497	0.00073	0.00006
	1	0.15326	−0.04526	0.01246	−0.00002	−0.00221	0.00095	0.00022	−0.00024	0.00000
	2	0.00090	0.01161	−0.00281	−0.00036	0.00034	−0.00008	0.00001	0.00002	−0.00002
	3	0.00014	0.00017	0.00034	−0.00016	−0.00003	0.00003	0.00000	0.00000	0.00000
0.5	0	−1.24823	0.50909	−0.39434	0.17389	−0.04870	0.01302	−0.00460	0.00107	0.00006
	1	0.14175	−0.05712	0.01147	0.00144	−0.00162	0.00073	0.00000	−0.00022	0.00008
	2	0.00048	0.01052	−0.00324	−0.00023	0.00044	−0.00008	−0.00001	0.00001	−0.00001
	3	0.00012	0.00015	0.00030	−0.00017	−0.00001	0.00004	−0.00001	0.00000	0.00000
0.1	0	−1.20477	0.56346	−0.38027	0.17029	−0.05227	0.01300	−0.00377	0.00115	−0.00016
	1	0.12723	−0.06839	0.01317	0.00311	−0.00178	0.00030	−0.00003	−0.00010	0.00010
	2	0.00010	0.00914	−0.00359	0.00006	0.00053	−0.00014	−0.00004	0.00002	0.00000
	3	0.00010	0.00013	0.00024	−0.00018	0.00001	0.00004	−0.00001	0.00000	0.00000
0.2	0	−1.14962	0.62013	−0.37335	0.16336	−0.05416	0.01426	−0.00326	0.00084	−0.00027
	1	0.10934	−0.07650	0.01790	0.00361	−0.00283	0.00018	0.00022	−0.00005	0.00001
	2	−0.00015	0.00744	−0.00374	0.00055	0.00048	−0.00025	−0.00001	0.00004	−0.00001
	3	0.00007	0.00012	0.00017	−0.00017	0.00004	0.00003	−0.00002	0.00000	0.00001

the second and third terms on the left-hand side of Eq. (14) are now treated as higher-order terms because of the factor ε by which they are multiplied.

On substituting the expansion (21) into Eqs. (14)–(19), and formally arranging terms of the same order in ε, the boundary value problem for the leading-order solution $\hat{f}_{(0)}$ becomes

$$\zeta_\rho \cos\theta_\zeta \frac{\partial \hat{f}_{(0)}}{\partial y} = \frac{1}{k} \hat{J}(\hat{f}_{(0)}, \hat{f}_{(0)}), \tag{B1}$$

together with Eqs. (28)–(30). The only difference from Sec. III C is that the operator $\mathcal{D}_\varepsilon$ is replaced by $\cos\theta_\zeta \partial/\partial y$. If Eqs. (B1) and (28)–(30) are rewritten in terms of the original variables ζ_r, ζ_θ, and ζ_z, then this boundary value problem is of the same form as that of a gas between plane parallel walls at rest; ζ_r, ζ_θ, and ζ_z correspond to the rectangular components of $\boldsymbol{\zeta}$, and ζ_r corresponds to the component normal to the wall. The solution $\hat{f}_{(0)}$ is an equilibrium state at rest (31).

The boundary value problem for the first-order solution $\hat{f}_{(1)}$ is

$$\zeta_\rho \cos\theta_\zeta \frac{\partial \hat{f}_{(1)}}{\partial y} = \frac{2}{k} \hat{J}(\hat{f}_{(0)}, \hat{f}_{(1)}) - \zeta_\rho \sin\theta_\zeta \frac{\partial \hat{f}_{(0)}}{\partial \theta}, \tag{B2}$$

together with Eqs. (39)–(41). The only difference from Sec. III C is that the operator $\mathcal{D}_\varepsilon$ is replaced by $\cos\theta_\zeta \partial/\partial y$. The curvature term $-\zeta_\rho \sin\theta_\zeta \partial \hat{f}_{(0)}/\partial\theta_\zeta$, which ought to appear in this equation, vanishes because the leading-order solution (31) is independent of θ_ζ. The boundary value problem for ϕ [Eq. (42)] is

$$\zeta_\rho \cos\theta_\zeta \frac{\partial \phi}{\partial y} = \frac{\hat{p}_{(0)}}{k} \mathcal{L}(\phi) - \zeta_\rho \sin\theta_\zeta \frac{1}{\hat{p}_{(0)}} \frac{d\hat{p}_{(0)}}{d\theta}, \tag{B3}$$

TABLE II. Coefficients c_{Cmn} in Eq. (C1) (BGKW model).

ε	m	$n=0$	1	2	3	4	5	6	7	8
+0	0	0.58171	0.05909	−0.00962	−0.00334	0.00182	−0.00009	−0.00020	0.00007	0.00000
	1	−0.07839	−0.05291	0.01063	0.00240	−0.00187	0.00024	0.00018	−0.00009	0.00001
	2	−0.00323	−0.00599	−0.00082	0.00094	−0.00001	−0.00015	0.00004	0.00001	−0.00001
	3	−0.00009	−0.00019	−0.00018	0.00001	0.00005	−0.00001	−0.00001	0.00000	0.00000
0.025	0	0.60379	0.08480	−0.00297	−0.00455	0.00038	−0.00030	0.00001	0.00017	−0.00002
	1	−0.07188	−0.04347	0.01366	0.00232	−0.00229	0.00009	0.00020	−0.00005	0.00002
	2	−0.00306	−0.00557	−0.00045	0.00105	−0.00004	−0.00018	0.00003	0.00002	−0.00001
	3	−0.00010	−0.00021	−0.00017	0.00003	0.00005	−0.00001	−0.00001	0.00000	0.00000
0.05	0	0.61594	0.09510	−0.00344	−0.00665	0.00007	0.00016	0.00019	0.00009	−0.00009
	1	−0.06746	−0.03775	0.01444	0.00150	−0.00260	0.00019	0.00029	−0.00005	−0.00001
	2	−0.00290	−0.00519	−0.00020	0.00104	−0.00010	−0.00019	0.00004	0.00002	−0.00001
	3	−0.00010	−0.00020	−0.00015	0.00004	0.00005	−0.00002	−0.00001	0.00000	0.00000
0.1	0	0.63178	0.10475	−0.00649	−0.00900	0.00062	0.00084	0.00013	−0.00009	−0.00010
	1	−0.06067	−0.02962	0.01459	0.00003	−0.00272	0.00050	0.00036	−0.00011	−0.00004
	2	−0.00262	−0.00458	0.00013	0.00096	−0.00021	−0.00017	0.00007	0.00002	−0.00002
	3	−0.00010	−0.00019	−0.00012	0.00005	0.00004	−0.00002	−0.00001	0.00001	0.00000
0.2	0	0.64895	0.10864	−0.01253	−0.00997	0.00231	0.00116	−0.00032	−0.00017	0.00005
	1	−0.05090	−0.01923	0.01325	−0.00195	−0.00224	0.00096	0.00023	−0.00021	0.00000
	2	−0.00220	−0.00369	0.00047	0.00073	−0.00032	−0.00010	0.00010	0.00000	−0.00002
	3	−0.00009	−0.00016	−0.00008	0.00006	0.00002	−0.00003	0.00000	0.00001	0.00000

together with Eqs. (44) and (45). Consequently, the solution $\hat{f} = \hat{f}_{(0)} + \hat{f}_{(1)}\varepsilon$ up to the first order is given by

$$\hat{f}(y, \theta, \boldsymbol{\zeta}) = \hat{p}_{(0)}E\left\{1 + \varepsilon\left[\frac{1}{\hat{p}_{(0)}}\frac{d\hat{p}_{(0)}}{d\theta}\Phi_{\mathrm{P}}\left(y, \boldsymbol{\zeta}; \frac{k}{\hat{p}_{(0)}}, \alpha_a(\theta)\right) + u_w\Phi_{\mathrm{C}}\left(y, \boldsymbol{\zeta}; \frac{k}{\hat{p}_{(0)}}, \alpha_a(\theta)\right)\right]\right\}.$$

(B4)

The functions $\Phi_{\mathrm{P}}(y, \boldsymbol{\zeta}; \tilde{k}, \alpha)$ and $\Phi_{\mathrm{C}}(y, \boldsymbol{\zeta}; \tilde{k}, \alpha)$ are the solutions of the following boundary value problems: for Φ_{P},

$$\zeta_\rho \cos\theta_\zeta \frac{\partial\Phi_{\mathrm{P}}}{\partial y} - \frac{1}{\tilde{k}}\mathcal{L}(\Phi_{\mathrm{P}}) = -\zeta_\rho \sin\theta_\zeta,$$

(B5)

$$\Phi_{\mathrm{P}} = (1 - \alpha)\Phi_{\mathrm{P}}(\tilde{\theta}_\zeta) \quad (y = 0, \cos\theta_\zeta > 0),$$

(B6)

$$\Phi_{\mathrm{P}} = 0 \quad (y = 1, \cos\theta_\zeta < 0),$$

(B7)

and for Φ_{C},

$$\zeta_\rho \cos\theta_\zeta \frac{\partial\Phi_{\mathrm{C}}}{\partial y} - \frac{1}{\tilde{k}}\mathcal{L}(\Phi_{\mathrm{C}}) = 0,$$

(B8)

$$\Phi_{\mathrm{C}} = (1 - \alpha)\Phi_{\mathrm{C}}(\tilde{\theta}_\zeta) \quad (y = 0, \cos\theta_\zeta > 0),$$

(B9)

$$\Phi_{\mathrm{C}} = 2\zeta_\rho \sin\theta_\zeta \quad (y = 1, \cos\theta_\zeta < 0).$$

(B10)

The only difference from Eqs. (A1)–(A3) and Eqs. (A4)–(A6) is that $\mathcal{D}_\varepsilon$ is replaced by $\cos\theta_\zeta \partial/\partial y$. To distinguish between these solutions, they are denoted by Φ_{P} and Φ_{C} without ε. Note that the boundary value problem (B5)–(B7) is of the same form as that of plane Poiseuille flow between parallel planes if it is written in terms of the original variables ζ_r, ζ_θ, and ζ_z and $(\zeta_r, \zeta_\theta, \zeta_z)$ are interpreted as the rectangular components of the molecular velocity. Similarly, the boundary value

problem (B8)–(B10) is of the same form as that of plane Couette flow between parallel planes. This is why the present solution is called the plane lubrication model. Substituting the distribution function (B4) into the mass conservation law, Eq. (52) is obtained.

The normalized flow velocities u_P and u_C and the normalized shear stresses S_P and S_C are given, respectively, by Eqs. (A8) and (A9) in which $\Phi_{J\varepsilon}$ is replaced by Φ_J. The mass flow rate coefficients $m_P(\tilde{k}, \alpha)$ and $m_C(\tilde{k}, \alpha)$ are given by

$$m_J(\tilde{k}, \alpha) = \int_0^1 u_J(y; \tilde{k}, \alpha)\, dy \quad (\text{J = P and C}). \tag{B11}$$

The $m_{P\varepsilon}$ and $m_{C\varepsilon}$ coincide with m_P and m_C, respectively, when $\varepsilon = +0$.

The macroscopic variables are given by the same formulas as those for the improved lubrication model in Sec. III D except that $u_{P\varepsilon}$, $u_{C\varepsilon}$, and so on, are replaced by u_P, u_C, and so on, respectively. For example, the flow velocity $\hat{v}_\theta$ is given by

$$\hat{v}_\theta = \varepsilon \left[\frac{1}{\hat{p}_{(0)}} \frac{d\hat{p}_{(0)}}{d\theta} u_P\left(y; \frac{k}{\hat{p}_{(0)}}, \alpha_a(\theta)\right) + u_w u_C\left(y; \frac{k}{\hat{p}_{(0)}}, \alpha_a(\theta)\right) \right]. \tag{B12}$$

APPENDIX C: DATABASE OF THE FUNCTIONS $m_{P\varepsilon}$ AND $m_{C\varepsilon}$

A simple database of the functions $m_{P\varepsilon}(\tilde{k}, \alpha)$ and $m_{C\varepsilon}(\tilde{k}, \alpha)$ in Eq. (A10) is provided here. This database is based on Chebyshev interpolation for two independent variables $\tilde{k}$ and α; it is a straightforward extension of that in Ref. [14]. The formula for $m_{J\varepsilon}(\tilde{k}, \alpha)$ (J = P and C) that is valid in the domain $0.05 \leqslant \tilde{k} \leqslant 20$ and $0.5 \leqslant \alpha \leqslant 1$ is given by

$$m_{J\varepsilon}(\tilde{k}, \alpha) = \sum_{m=0}^{M-1} \sum_{n=0}^{N-1} c_{Jmn} T_m(A \ln \alpha + 1) T_n(B \ln \tilde{k}) \quad (\text{J = P and C}). \tag{C1}$$

Here, $M = 4$, $N = 9$, $A = 2/(\ln 2)$, $B = 2/(\ln 400)$, and the constants c_{Pmn} and c_{Cmn} for the BGKW model are tabulated in Tables I and II, respectively. The $T_n(\cdot)$'s are the Chebyshev polynomials defined by $T_0(t) = 1$, $T_1(t) = t$, and $T_n(t) = 2t T_{n-1}(t) - T_{n-2}(t)$ $(n = 2, 3, \dots)$. The functions $m_P(\tilde{k}, \alpha)$ and $m_C(\tilde{k}, \alpha)$ in Eq. (B11) are generated simply using the data for $\varepsilon = +0$. A comparison with the results of direct calculations of Eq. (A10) shows that the error of the formula (C1) is less than 0.02% uniformly in the domain $0.05 \leqslant \tilde{k} \leqslant 20$ and $0.5 \leqslant \alpha \leqslant 1$.

[1] G. Karniadakis, A. Beskok, and N. Aluru, *Microflows and Nanoflows: Fundamentals and Simulation* (Springer, New York, 2005).

[2] C. Cercignani, *Slow Rarefied Flows* (Birkhäuser, New York, 2006).

[3] Y. Sone, *Molecular Gas Dynamics* (Birkhäuser, New York, 2007).

[4] C. Shen, *Rarefied Gas Dynamics* (Springer, New York, 2010).

[5] F. Sharipov, *Rarefied Gas Dynamics* (Wiley-VCH, New York, 2016).

[6] A. Burgdorfer, The influence of the molecular mean free path on the performance of hydrodynamic gas lubricated bearings, ASME J. Basic Eng. **81**, 94 (1959).

[7] R. F. Gans, Lubrication theory at arbitrary Knudsen numbers, ASME J. Tribol. **107**, 431 (1985).

[8] S. Fukui and R. Kaneko, Analysis of ultra-thin gas film lubrication based on linearized Boltzmann equation: First report—derivation of a generalized lubrication equation including thermal creep flow, ASME J. Tribol. **110**, 253 (1988).

[9] T. Veijola, H. Kuisma, and J. Lahdenperä, The influence of gas-surface interaction on gas-film damping in a silicon accelerometer, Sens. Actuators A **66**, 83 (1998).

[10] S. C. Kang, R. M. Crone, and M. S. Jhon, A new molecular gas lubrication theory suitable for head-disk interface modeling, J. App. Phys. **85**, 5594 (1999).

[11] P. Bahukudumbi and A. Beskok, A phenomenological lubrication model for the entire Knudsen regime, J. Micromech. Microeng. **13**, 873 (2003).

[12] Reference [3], Sec. 4.3.

[13] T. Doi, A model of micro lubrication between two walls with an arbitrary temperature difference based on kinetic theory, Phys. Fluids **32**, 052005 (2020).

[14] T. Doi, A model of micro lubrication between two walls with unequal temperature distribution based on kinetic theory, Phys. Fluids **33**, 032014 (2021).

[15] H. G. Elrod, A derivation of the basic equations for hydrodynamic lubrication with a fluid having constant properties, Q. Appl. Math. **17**, 349 (1960).

[16] P. L. Bhatnagar, E. P. Gross, and M. Krook, A model for collision processes in gases. I. Small amplitude processes in charged and neutral one-component systems, Phys. Rev. **94**, 511 (1954).

[17] P. Welander, On the temperature jump in a rarefied gas, Ark. Fys. **7**, 507 (1954).

[18] H. Sugimoto and Y. Sone, Numerical analysis of steady flows of a gas evaporating from its cylindrical condensed phase on the basis of kinetic theory, Phys. Fluids A **4**, 419 (1992).

[19] Y. Sone, New kind of boundary layer over a convex solid boundary in a rarefied gas, Phys. Fluids **16**, 1422 (1973).

[20] Y. Sone and S. Takata, Discontinuity of the velocity distribution function in a rarefied gas around a convex body and the S layer at the bottom of the Knudsen layer, Transp. Theory Stat. Phys. **21**, 501 (1992).

[21] T. Doi, Effect of weak gravitation on the plane Poiseuille flow of a highly rarefied gas, Z. Angew. Math. Phys. **63**, 1091 (2012),

[22] P. G. Drazin and W. H. Reid, *Hydrodynamic Stability* (Cambridge University Press, Cambridge, 1981), Sec. 18.

[23] T. Doi, Flows of a rarefied gas between coaxial circular cylinders with nonuniform surface properties, Open J. Fluid Dyn. **9**, 22 (2019).

[24] C. K. Chu, Kinetic-theoretic description of the formation of a shock wave, Phys. Fluids **8**, 12 (1965).